

# Textural mapping and building a paragenetic interpretation of hydrothermal veins



Shane Webb, Taija Torvela\*, Rob Chapman and Lucia Savastano

Ores and Mineralisation Group, School of Earth and Environment, University of Leeds, UK

TT, 0000-0003-1539-8755

\*Correspondence: [t.m.torvela@leeds.ac.uk](mailto:t.m.torvela@leeds.ac.uk)

**Abstract:** Paragenetic interpretation, defined as the process of constraining the order in which the phases (minerals) comprising a rock formed, are fundamental in all disciplines requiring a detailed mapping of the genetic relationships between the investigated crystal(s) and their surrounding phases. Ore geology, geochronology, petrological and fluid inclusion studies are underpinned by a robust interpretation of the paragenesis. Without this understanding, the interpretation of the analytical data will be greatly restricted and potentially wrong. Textural mapping is particularly useful for studying phases precipitated into hydrothermal veins because the host many metallic ore deposits. Understanding the paragenesis and the association of ore minerals feeds directly into the approach taken towards exploration, mining operation and ore processing. Apart from ore deposits, precipitation of hydrothermal phases occurs in any setting where hot fluids interact with rock or sediment (e.g. CCS storage; geothermal facilities). This paper summarizes the principles for developing a robust paragenetic interpretation, including demonstrating the practical workflow via a case study from a sulfide-bearing vein near Loch Tay, Scotland. The principles and the workflow outlined in this paper are applicable to any discipline and route of investigation that necessitates a robust understanding of the relationships of the phases in a rock.

Paragenesis is defined as the ‘association of minerals in rocks and rock suites in relation to their origin’ (Bowes 1989). The first recorded use of the term ‘paragenesis’ was by the German mineralogist August Breithaupt (1849: *Die Paragenesis der Mineralien*). The etymology of the word comes from the Greek phrase for ‘born beside’, and in petrological studies, the application of paragenesis typically pertains to the process of constraining the order in which the phases (minerals) comprising a rock or vein formed (e.g. Kamilli 1998). Phases in a rock can form via the following processes: a single progressive episode of crystallization (e.g. fractional crystallization of magma); precipitation/crystallization from repeated fluid or magma injections separated by intervals of non-deposition (e.g. hydrothermal veins); during the progressive metamorphic evolution of a rock volume; or a combination of these.

The aim of all paragenetic studies is to establish the context of phases in a sample; this guides various subsequent analytical studies and the interpretation of the data acquired from them. Although the word ‘paragenesis’ in principle may be applied to any material from the Earth that shows evidence of multiple or progressive phases of crystallization or precipitation, the most common usage of the term is perhaps within the field of ore geology and, in particular, in the context of hydrothermal veins (e.g. Kamilli 1998; Tadesse 2004; Monteiro

*et al.* 2007; van Ryt *et al.* 2017; Mansurbeg *et al.* 2020). Precipitation of different phases at different times (either via multiple fluid injection events or progressively) often occurs in hydrothermal ore deposits as a result of variations in pore fluid pressure, the temperature or chemical composition of the hydrothermal solution, or a combination of these processes. In ore geology, understanding the paragenesis facilitates the correlation of the metal (s) with distinct fluid episodes and their characteristic phase assemblages, which can then be used to formulate strategies for geochemical exploration. Paragenetic information can also give circumstantial indications of processes that may affect the grade of a deposit. For example, later fluid episodes post-dating an initial mineralization stage may be associated with dissolution and downgrading of a prospect, or conversely, remobilization and concentration of the metal to augment the grade (Hastie *et al.* 2020). An important by-product of describing the paragenesis is a superior understanding of the mineralogical characteristics of the deposit, which can have implications for processing the extracted ore (Gregory *et al.* 2013; Sykora *et al.* 2018; Müller and Ehle 2021). For example, documenting the paragenesis of the Pebble Cu-Mo-Au deposit in Alaska (USA) led to the revelation that, whilst some of the gold was hosted within chalcopyrite, a significant amount occurs within pyrite and

From: Butler, R. W. H., Torvela, T. and Williams, L. (eds) *Geological Mapping of Our World and Others*. Geological Society, London, Special Publications, **541**, <https://doi.org/10.1144/SP541-2023-17>

© 2023 The Author(s). This is an Open Access article distributed under the terms of the Creative Commons Attribution License (<http://creativecommons.org/licenses/by/4.0/>). Published by The Geological Society of London.

Publishing disclaimer: [www.geolsoc.org.uk/pub\\_ethics](http://www.geolsoc.org.uk/pub_ethics)

consequently different ore processing approaches may be required (Gregory *et al.* 2013).

Paragenetic analyses are, however, fundamental not only in ore geology and hydrothermal vein studies: robustly performed research into diagenetic studies, rock alteration, geochronology and fluid inclusions is underpinned by a detailed understanding of the relationships between the investigated crystal(s) and their surrounding phases. For example, Fulignati (2020) emphasized the importance of constraining the paragenesis of clay minerals as a means of describing the physiochemical conditions (temperature and pH) of the environment in which the alteration developed. In geochronology, paragenetic interpretations allow radiometric ages, obtained from phases crystallized or precipitated within the studied rock volume, to be tied to specific episodes in the geological history. It is, therefore, common for researchers to publish geochronological ages within the framework of a paragenetic sequence (e.g. deMelo *et al.* 2016; Babo *et al.* 2017; Fan *et al.* 2021; Myint *et al.* 2021). For example, Li and Vasconcelos (2002) noted the importance of constraining the paragenetic context of dateable minerals in their attempts to unravel the palaeoclimatic conditions in Central Australia during the Oligocene–Miocene transition. Paragenetic studies are similarly important for constraining the context of fluid inclusions; a robust linkage of the observed inclusions to the paragenesis allows for the homogenization temperatures and geochemical characteristics derived from the inclusions to be linked directly to a specific phase assemblage and episode of fluid flow (e.g. Imai 2000; Moura *et al.* 2014; Soloviev and Kryazhev 2018; Mehrabi *et al.* 2019). In metamorphic petrology and microstructural analysis, the interpretation of the relationships of the mineral assemblages, their metamorphic and/or melting reactions and equilibrium textures (or lack thereof) is, technically, a form of paragenetic interpretation that underpins a variety of studies, e.g. palaeostress analysis and geothermobarometry for establishing the deformational and metamorphic history of the rock (e.g. Vidal *et al.* 2006; Pittarello *et al.* 2012; Lanari *et al.* 2014; Lee *et al.* 2020; Gilio *et al.* 2021).

The conceptual development of paragenetic analysis in the nineteenth century was made possible by the construction of the first polarizing microscope by Giovanni Battista Amici in 1833 (Rochow and Tucker 1994). Initially, paragenetic observations were made chiefly with either a transmitted (polarized) light microscope or, in the case of metallic ore deposits, with a reflected light microscope. In the absence of quantitative mineralogical analysis tools, the earlier publications that reference paragenesis were qualitative and descriptive, particularly in the nineteenth century and well into the twentieth century (e.g. Gruner 1922; Brammall *et al.* 1937;

Keys 1940; Sims 1956). The papers generally focused on informing readers of the cross-cutting relationships of the phases, i.e. the order in which the minerals formed, and most contained little (if any) interpretation about the wider geological implications of the paragenetic sequence. For example, Pumpelly (1871) simply catalogued the paragenesis of two copper veins around Lake Superior. Finlayson (1910) was one of the first authors to attempt a regional paragenetic assessment: he described the paragenesis of lead-zinc-copper ores throughout the British Isles and concluded that the sulfides, regardless of their location, show consistent paragenetic relationships. Similar studies began to emerge elsewhere at this time: e.g. Ray (1914) used a reflected light microscope to study over 500 specimens collected from various mines throughout the Butte District of Montana, interpreting that the precipitation of pyrite induced the formation of chalcopyrite. These and other similar early papers demonstrate that authors were beginning to develop an awareness of the regional and sequential nature of the hydrothermal processes that are associated with different ore deposits.

The advent of more sophisticated, quantitative analytical instrumentation along with the growing realization that many geological systems were paragenetically complex led to the design of more advanced studies. With the introduction of techniques such as Laser-Raman spectroscopy, Laser-Ablation – Inductively-Coupled Plasma Mass Spectrometry (LA-ICP-MS) and Electron Probe Microanalysis (EPMA), it became possible to derive detailed (trace) element and (stable) isotope data from almost any phase in a rock (e.g. Engel *et al.* 1958; Taylor 1974; Randive *et al.* 2022). The advances in the analytical capabilities and the quality of the ensuing observations required robust links to be made between the samples and phases being analysed and their textural and geological context. Consequently, paragenesis began to be discussed as part of both the analytical and the wider geological setting, with researchers increasingly relating the interpretation of their quantitative analytical data to paragenetic interpretations and the regional geological history (e.g. Hagni and Grawe 1964; Kelly and Turneaure 1970; Richardson and Pinckney 1984).

The commercialization of the Scanning Electron Microscope (SEM) in 1965 addressed the problem of routinely and easily combining detailed geochemical and spatial (i.e. visual) data. The proliferation of SEM marked a significant improvement in our capability to link textural observations with quantitative compositional data (e.g. McMullan 2006). Today, SEMs include a range of tools such as Back-Scatter Electron Microscopy (BSE), Energy Dispersive X-ray Spectroscopy (EDS or EDX), cathodoluminescence (CL), and Electron Back-Scatter

## Textural mapping and building a paragenetic interpretation

Diffraction (EBSD). These allow for visual phase mapping at a micron scale, along with the capability to simultaneously acquire semi-quantitative geochemical data of the composition of the different phases and their crystallographic textures, including discrete zoning in individual grains. For example, some phases (e.g. hydrothermal vein quartz) appear to be homogenous to the naked eye, but the CL technique has revealed that they may be comprised of several distinct generations (Fig. 1a; e.g. Marshall 1988; Machel 2000; Götze *et al.* 2001; Landtwing and Pettke 2005). The incorporation of SEM techniques has led to paragenetic interpretations becoming more robust by providing a detailed and powerful context against which to consider other analytical results.

This paper will summarize the key principles of textural mapping and what textural evidence can be used towards developing a paragenetic interpretation. Our examples come mostly from metal-bearing hydrothermal veins but the fundamental considerations and principles of spatial relationships between phases are largely applicable to any paragenetic study. After describing the theoretical principles, we will demonstrate a practical workflow for developing a robust paragenetic interpretation with a case study from a small Au–Ag–Cu–Pb–Zn vein in Glen Almond, south of Loch Tay, Scotland.

### Samples and instrumentation in paragenetic studies

In this section, we briefly summarize some key considerations when planning a sampling campaign for a paragenetic study, and discuss the most common instruments used in paragenetic analysis. Spatial relationships can be established at several scales, from naked-eye outcrop observations to micro- and even nano-scale data, but in paragenetic studies observations are typically made at microscale. In modern research, the traditional microscopy techniques are supplemented by more detailed and semi-quantitative electron optics. The Scanning Electron Microscope (SEM) is, in particular, the most commonly used instrument in paragenetic studies as it enables relatively fast and cost-efficient way of gaining very detailed textural and compositional semi-quantitative data. Basic SEM techniques can, if necessary, be complemented by more detailed quantitative microstructural or microchemical analyses using e.g. Electron Backscatter Diffraction in SEM, Electron Microprobe Analyser, or Laser-Ablation Inductively-Coupled Plasma Mass Spectrometry (e.g. Combes *et al.* 2021; Perret *et al.* 2021), but SEM is normally sufficient for establishing a robust textural analysis. However, classical microscopy still forms an important first step in any sample

characterization and can, in some cases, be sufficient to formulate a good paragenetic interpretation. Paragenetic relationships can be established at several scales, and spatial relationships can in some cases be established either at outcrop or by eye from sections of samples or core.

### Sample collection, sample representativeness and scale of observation

The number and volume of samples depends on the specific aims of the study and the geological context but sample representativeness must be carefully considered. Most studies are constrained by the number of observations that can be feasibly made, and it is therefore imperative that the sample suite(s) are as representative of the whole system as possible. If structural interpretation is required (e.g. interpretation of shape fabrics with transmitted light microscopy, or EBSD analysis of crystallographic textures), the samples must be orientated. Furthermore, the three-dimensional nature (textural anisotropy) of many geological materials needs to be taken into account.

The paragenesis is typically determined through examination of polished thin-sections or resin blocks. The representativeness of a single thin section/block decreases rapidly with the increase in the studied rock volume and/or textural anisotropy. For example, it is not uncommon for vein and dyke systems to be hundreds of meters or even many kilometres long, with individual vein/dyke widths in the order of several metres (Higgins 1985; Plumlee and Whitehouse-Veaux 1994; Wang *et al.* 2021). Such veins form via repeated fracturing-sealing cycles where the fluid properties and precipitated phases may or may not change over time (Fig. 1b; Sibson 1994). The spatial evolution of the fracture porosity and, consequently, the distribution of the precipitated phases in such a multi-generational vein system is, therefore, inherently texturally anisotropic and heterogeneous. This is famously demonstrated by the so-called ‘nugget effect’ in vein-hosted gold deposits, where large volumes of the vein system are barren or lower grade, interrupted by smaller high-grade volumes (e.g. Dominy *et al.* 2001). The heterogeneous distribution of phases precipitated during multiple fluid injection events poses inevitable challenges to sample representativeness. The crystal sizes in many rocks, including veins and dykes can also be quite large (cm-scale to m-scale) particularly in rapidly de-pressurizing, or undercooled fluid systems such as pegmatites (e.g. Butler and Torvela 2018). Large crystal sizes severely reduce the representativeness of a single sample or thin section.

A reasonably robust approach to large vein systems can be achieved via a systematic approach to

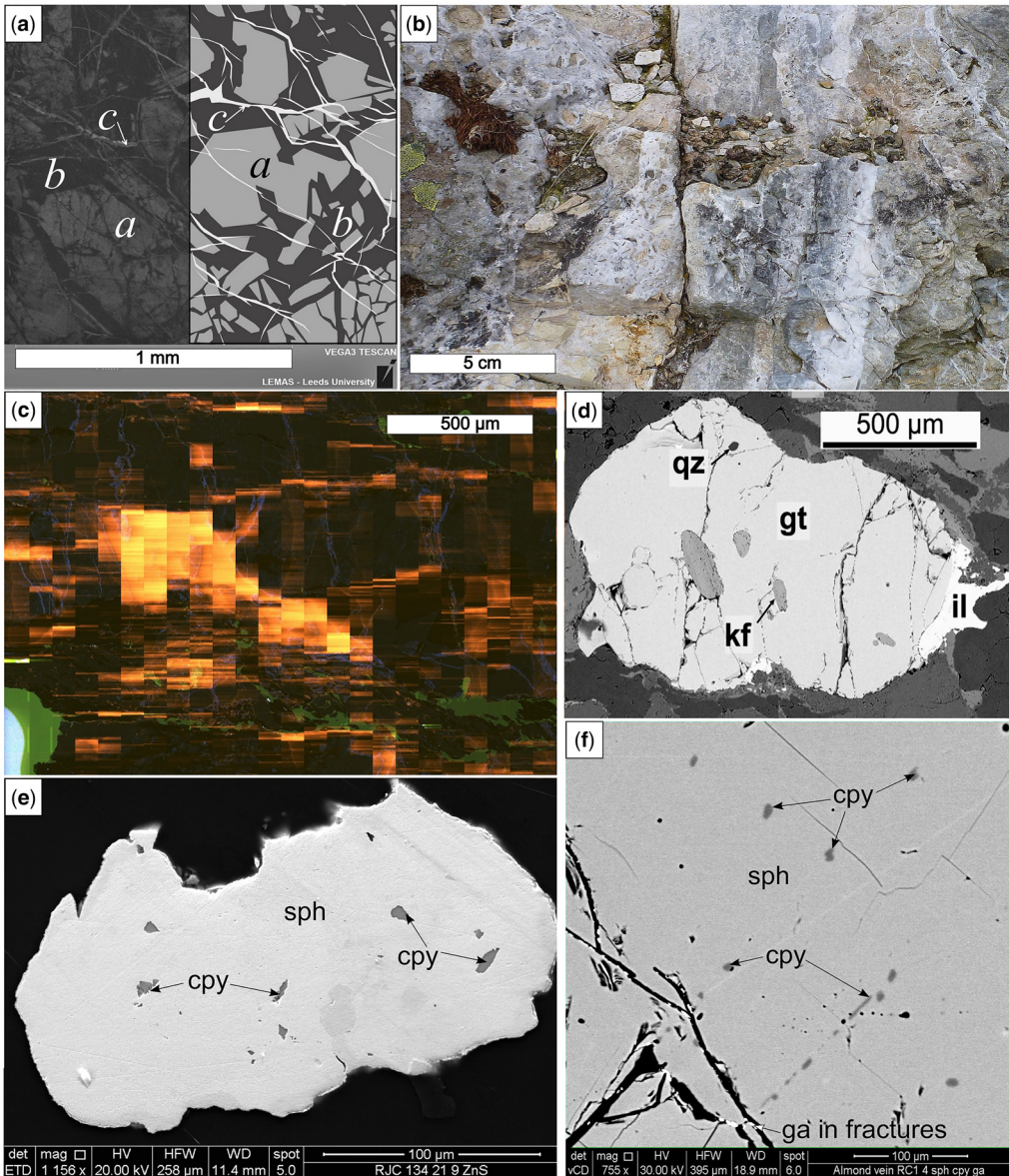


**Fig. 1.** Examples of various textures used in paragenetic interpretation. These images showcase the importance of understanding the underlying geological process that resulted in the observed textures, as each will imply different number of events. **(a)** Law of cross-cutting relationships, illustrated by a panchromatic SEM-CL image (left) and its line drawing (right) of three different quartz generations in a quartz vein near Aberfeldy, Scotland. The occasionally zoned but dominantly CL-light grey, angular quartz *a* is brecciated by the CL-dark grey/black quartz *b*; both are cross-cut by the thin, CL-light grey quartz veins *c*. In this example, therefore, the law of cross-cutting relationships dictates that the zoned quartz is interpreted as the oldest phase; followed by a brecciation event with quartz *b*; with *c* being the youngest. **(b)** Part of a >2 m thick layered vein at Lead Trial, Loch Tay, Scotland. The vein is clearly layered, probably as a result of repeated fracturing-sealing episodes, with the individual breccia layers all showing slightly different mineral assemblages, colours and textures. Note also the hydrothermal breccia on the left-hand side of the image, further evidence of multiple fluid injection and fracture opening events. In this case, it will be very difficult to determine the sequence of deposition in most of the layers, although some cross-cutting relationships can be observed. In addition, this is a good example of problems with sample representativeness: the area of a single thin section is not representative of the variations within the vein. **(c)** An extreme example of smearing of the CL caused

## Textural mapping and building a paragenetic interpretation

the pre-sampling characterization of the sampled rock, in order to capture those parts of the system that are assessed to be representative. This will require detailed field observations on vein mineralogy, structures and textures, including any obvious compositional or textural zonation or other anisotropies. Sampling and subsequent micro-scale analysis must, therefore, always be underpinned by developing an understanding of the field relationships and characteristics of sampled rocks in as much detail as is reasonably possible. It is normally necessary to sample several parts of the representative rock volume and prepare multiple thin sections/blocks representing a single rock sample. Nevertheless, the scale of thin sections compared to the size of a typical geological system means that it may not be possible to observe the complete set of interactions between specific fluid/melt generations and mineral phases. A critical assessment of uncertainties must be incorporated into any paragenetic interpretation and its implications.

### *Transmitted light and reflected light microscopy*

Whilst undertaking analyses using an SEM is now the standard approach for detailed paragenetic studies, this facility may not always be available. However, the principles of textural mapping, outlined later in this paper, are equally applicable in 'classical' microscopic studies. Furthermore, any SEM analyses (or other microanalytical investigations) should always be preceded by a careful recording, including initial hand sketches, photography and scanning of the polished thin sections using traditional transmitted light microscopy (and reflected light microscopy, where appropriate). This serves two important purposes: (i) observations of the overall mineralogy, grain sizes, initial observations and interpretations of the paragenesis and the general context of the phases of interest will greatly inform and guide the microanalytical investigations, facilitating efficient usage of equipment time; and (ii) photographs of the areas of interest, and scans or

photographic montages of entire thin sections, both in plane polarized and cross-polarized light, provide extremely useful maps for navigating the thin sections whilst using the microanalytical equipment, again facilitating efficient equipment usage. In addition, the sections need to be carbon-coated for SEM; a detailed and complete classical microscope study ahead of SEM characterization eliminates the need for the extra step of removing the carbon coating.

Transmitted light microscopy (TLM) is a generic term pertaining to any form of microscopic study involving transmission of light from below the specimen, through the polished thin section and into the objective lens where the image is produced (Köhler 1894; Oldenbourg 2013). TLM is frequently used in geological sciences for the study of non-opaque minerals, and it can be perfectly sufficient in textural mapping that involves relatively simple non-opaque mineralogy. TLM is also useful for a basic characterization of hydrothermal alteration (e.g. chlorite, feldspar and epidote-group minerals are all easily detectable with TLM). In addition, TLM is a cheap and reliable way of identifying obvious cross-cutting relationships between different phases. However, the usability of TLM is limited by its relatively low resolution and its inability to resolve the often subtle internal variations in mineral chemistry that are frequently observed in silicates, sulfides (e.g. the As content of Py and native metals in hydrothermal vein systems e.g. Thomas *et al.* 2011; Frelinger *et al.* 2015; Chapman *et al.* 2021; Combes *et al.* 2021). In addition, TLM cannot distinguish between opaque minerals.

Reflected light microscopy (RLM) is another relatively inexpensive standard method and it is particularly suitable for the examination of opaque minerals. The first reference to the use of reflected light to study opaque bodies was made in the mid-nineteenth century and RLM eventually became the most popular tool for ore mineral characterization from the 1950s onwards (Nuttall 1979). The basic process involves the illumination of a polished thin section from above with the objective lens (Davidson and Lofgren 1991). Opaque minerals are observed

---

**Fig. 1.** *Continued.* by the presence of carbonates in late fractures cross-cutting the earlier quartz generations. Locality cannot be disclosed for confidentiality reasons. (d) K-feldspar (kf) and quartz (qz) inclusions within garnet (gt) in a quartzo-feldspathic gneiss metamorphosed to upper amphibolite facies conditions. In this case, the inclusions are part of an older phase assemblage and the younger garnet grew around it during prograde metamorphism. Il = ilmenite. TLM image, modified from Lee *et al.* (2020). (e) An example of a texture showing inclusions, in this case chalcopyrite (cpy) inclusions within sphalerite (sph). Although the cpy is present as inclusions within the sph, both phases probably precipitated approximately coevally during a single fluid event rather than two separate events (see text). BSE image, Lead Trial, Loch Tay, Scotland. (f) An example of the 'chalcopyrite disease' (see text). The exsolution of chalcopyrite (cpy) and sphalerite (sph) results in small blebs and inclusion trails of cpy within the sph. Note how the phase boundaries are slightly more subtle than in the case of sequential co-precipitation of cpy and sph in D) and how the cpy forms an inclusion trail along a sph cleavage plane in the lower part of the picture. This texture requires only one precipitation event. The later fractures in the lower left-hand corner carry some BSE-bright galena; a second fluid event is needed for this later texture. Glen Almond, Scotland.

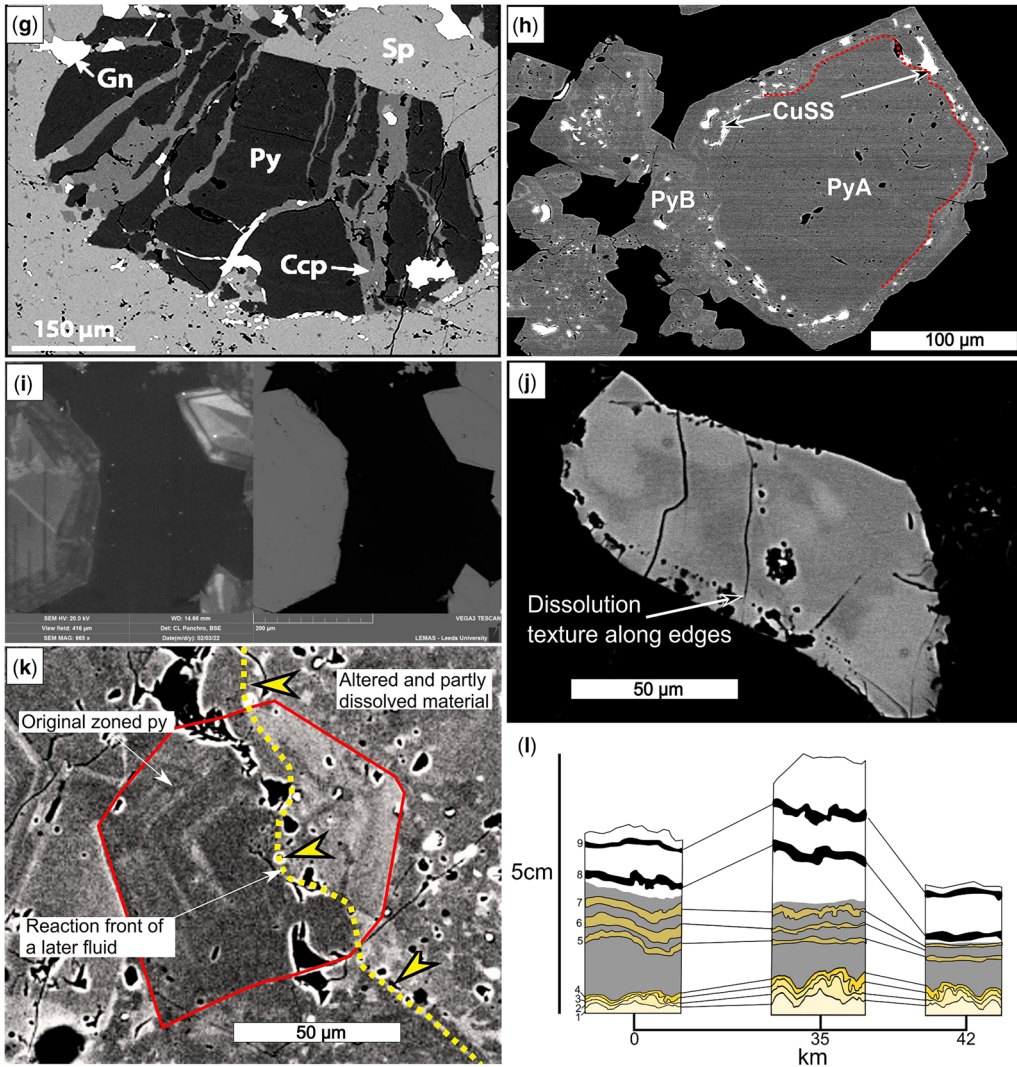


**Fig. 1. Continued.** (g) Sequential co-precipitation of sulfides during a single fluid event (see text). The pyrite (Py) is precipitated early but is fractured due to the rapidly changing physico-chemical ambient conditions, with subsequent precipitation of chalcopyrite (Ccp) and galena (Gn) into the pyrite fractures. The sphalerite (Sp) is probably also part of the same precipitation sequence although this image alone is insufficient to determine this with certainty. BSE image, KSM porphyry deposit, British Columbia. Photo credit: Hugh Graham. (h) Growth zoning in pyrite. The pyrite (PyA) in the core of the larger grain is relatively BSE-homogeneous (core-rim boundary partly outlined with a red stippled line). The core is surrounded by a rim that consists of an inclusion ring of a copper sulfosalt phase (CuSS) near interface with the featureless pyrite (BSE-bright phase) which is in turn interfingered and surrounded by another, more heterogeneous pyrite phase (PyB). These relationships imply at least two, possibly three, separate fluid events. Mount Milligan porphyry deposit, British Columbia. (i) Growth zoning in quartz crystals growing into a void (i.e. a vug) in a hydrothermal quartz vein. Note how the BSE image (right) is unable to resolve the internal structure of the quartz grains, clearly visible in the CL (left; see the methodology section for further information). This type of growth zoning occurs during a single, evolving fluid event due to slightly changing or fluctuating fluid compositions. The precipitating crystals are free to grow according to its natural crystal morphology. Had any subsequent precipitation of phases (quartz or other) into the vug occurred, these later phases would encompass the older, euhedral, zoned quartz grains without altering their morphology. However, interpreting the euhedral grains as the first to precipitate within the *entire* vein system may be erroneous as vugs can form at any stage of repeated vein opening and growth (see text). Lead Trial, Loch Tay, Scotland. (j) Alteration of a titanite grain in a quartzo-feldspathic, high-grade gneiss. The original titanite has been partially altered during retrograde metamorphism and associated

### Textural mapping and building a paragenetic interpretation

when light gets reflected back towards the lens by specular or diffuse mechanisms, producing an image in which different phases can be identified and studied (e.g. Sanderson 2019). By combining TLM observations with RLM observations, a relatively detailed mapping of the basic cross-cutting relationships of non-opaque and opaque phases can be conducted. However, like TLM, RLM resolution is relatively low compared to microanalytical techniques and is equally incapable of resolving most compositional zoning and detailed geochemical variations within crystals. Efficient usage of RLM also requires significant experience that can take years to develop, and differences in the ability of individual observers to perceive subtle colour changes can be a significant issue.

#### *SEM approaches involving CL, BSE, and EDX (EDS)*

The advantage of SEM approaches is the ability to image subtle variations in the crystallographic texture and compositional variations in individual crystals in much greater detail and resolution than is possible with TLM/RLM. There are various SEM tools that can be used, but for paragenetic mapping the most commonly used tools are CL, BSE and EDX.

The ‘bread-and-butter’ of SEM-facilitated textural mapping is the combination of Back-Scatter Electron (BSE) analysis and Energy Dispersive X-ray (EDX) Spectroscopy. The BSE detector records electrons emitted from the sample upon scanning; the backscattered electrons are used to create high-resolution images showing the distribution of different elements in a sample. The rate of production of backscattered electrons depends on the atomic number of the element being analysed; denser elements and, therefore, denser phases will deflect incoming electrons more strongly, producing brighter images (Niedrig 1978). BSE can resolve some zoning within individual crystals and it is commonly used in geochronological studies to identify zoning in dateable minerals such as zircon or titanite (e.g. Torvela and Kurhila 2022). EDX, on the other hand, generates semi-quantitative compositional

data for targets at a micron scale: in practice, EDX is used as a phase identification tool through comparison of the elemental spectrum of the target with known spectra for specific minerals. The combination of BSE and EDX provides a powerful analytical toolkit for detailed mineral identification and textural/compositional mapping.

Whilst BSE can be used to detect subtle compositional variations in some phases, the resolution of this technique is insufficient to enable a full range of observations on detailed mineral geochemistry. Cathodoluminescence (CL) can help in gaining more information of specific phases and their precipitation history. The CL technique is based on the emission of light from a mineral upon electron bombardment (Marshall 1988). Electrons are stimulated through the use of a hot filament and accelerated towards an anode. The electron beam scans across the sample and a specific CL detector, attached to the SEM, records the emitted light from the sample as a series of images (Götze and Kempe 2009). CL imaging for paragenetic mapping is particularly suitable for quartz: variations in quartz compositions are associated with impurities comprised of trace elements substituted into the mineral lattice, especially aluminium (Götze *et al.* 2001; Götze 2009; Stevens-Kalceff 2009; Frelinger *et al.* 2015). The specific element substituted depends on a wide range of factors such as crystallization rate, fluid composition, pressure, temperature and post-mineralization deformation (Götze and Möckel 2012). In the context of the paragenetic analysis of hydrothermal veins, commonly composed of multiple quartz generations injected at different times, the ability to image different quartz generations can greatly assist in developing a robust paragenetic interpretation and development history for the vein (Fig. 1a).

However, there are limitations to the resolution of CL in terms of its ability to distinguish between phase generations. The textural variations within quartz, for example, that are resolvable with CL are due to crystal lattice defects caused by trace element substitution, giving different CL responses (Götze *et al.* 2001; Götze 2009; Stevens-Kalceff 2009; Frelinger *et al.* 2015). Depending on the fluid source and fluid-rock interactions, it is possible that successive

---

**Fig. 1.** *Continued.* re-hydration of the amphibolite-facies gneisses, expressed by the BSE-lighter patchy zoning of the grain. Note also the partly dissolved, porous outer edge of the lower part of the grain. Greenschist-facies Karkkila shear zone, Finland. **(k)** An example of alteration and dissolution textures. A later fluid reacted chemically with the existing phases (mostly pyrite in this image), resulting in a mottled, diffuse appearance replacing the zoned, BSE-darker texture of the original pyrite (grain boundary outlined in red). The reaction front, outlined with the yellow stippled line, progressed from right to left as indicated by the arrows. In this case, the alteration reactions have also caused partial dissolution of the original pyrite, evidenced by the holes in the pyrite to the right of the reaction front whereas to the left, similar holes are absent within this pyrite grain. BSE image, modified from Hastie *et al.* (2020). **(l)** The principle of sphalerite stratigraphy. Modified from McLimans *et al.* (1980).

generations of quartz may not display sufficient variations in their trace element geochemistry, in which case CL will not be able to resolve the textural variability of the different generations. This could result in the interpreted paragenetic sequence for a given deposit being incomplete, or the incorrect conclusion that all of the quartz belongs to the same generation. In theory, this could be resolved through the coupled use of CL and LA-ICP-MS, which will enable the visualization of more detailed trace element variations within the section of quartz (or any other phase) that is being observed.

Another issue with CL analyses relates to the higher relative luminescence of carbonate minerals, particularly of calcite, compared to silicate minerals. The higher luminescence typically manifests itself as ‘smearing’ of the CL image (Fig. 1c). It may, therefore, not be possible to image carbonate-rich materials without reducing the brightness to the point that the internal textural features are lost. Reed and Milliken (2003) found that, in some cases, this problem can be at least partly resolved by using broadband short wavelength filter, which allows 80–90% transmissivity from 385 to 495 nm and minor transmissivity at 350 nm, to fire shorter wavelengths.

## Developing a paragenetic interpretation

The rest of the paper is divided into two parts in which we (1) summarize the basic approaches and principles underpinning textural mapping and a subsequent paragenetic interpretation; and (2) demonstrate a practical workflow for documenting observations and developing a robust paragenetic interpretation, via a small case study.

### *Part 1: basic principles of textural mapping*

The basic principles in this section are not necessarily instrument-specific and apply whether one uses sophisticated microanalytical methods or traditional optical microscopy. Whatever methodology is used, it should be reiterated that a robust sampling strategy, recording and description of observations at all stages, and communicating the observations to the reader via high-quality images, are crucial in order to justify the final interpretation of the paragenesis.

### *Crosscutting relationships and inclusions*

The law of crosscutting relationships is the fundamental tool for establishing the age relationship between geological features of any type. This concept is familiar to all geologists, and the importance of it was recognized already by Steno (1669) who stated, ‘*If a body or discontinuity cuts across a stratum, it must have formed after that stratum*’. The law

of crosscutting relationships applies at all scales, and it is ubiquitous in both field and paragenetic studies (Slack 1980; Haerberlin *et al.* 2004; Dewaele *et al.* 2006; Legros *et al.* 2016; Wei *et al.* 2019; Taylor *et al.* 2021). Observations of crosscutting relationships are crucial in determining the paragenesis of multi-generational veins (e.g. Taylor *et al.* 2021). In its most simple form, crosscutting relationships consist simply of an older material being intruded or fractured by younger material (Fig. 1a). Another geometric relationship arising from the law of crosscutting relationship is the ‘law of inclusions’ which stipulates that clasts or grains engulfed by other material are older than that surrounding material (Fig. 1d; Lyell 1833; Vaughan and Ixer 1980; Martínez-Abad *et al.* 2015; Andersen *et al.* 2016; Alford *et al.* 2020).

However, using cross-cutting relationships or inclusions to indicate the sequence of precipitation can be problematic in dynamically crystallizing systems and in systems where the fluid composition and/or the physico-chemical conditions of precipitation evolve. Hydrothermal vein systems in particular are slightly different in terms of the dynamic nature of their formation compared with most other geological features. Hydrothermal vein formation is characterized by extremely rapid fracture propagation and fluid depressurization that often (although not inevitably) results in phase separation and (partial) precipitation of crystals from the fluid and, consequently, progressive changes in the fluid chemistry and temperature (Sibson 1994; Quilichini *et al.* 2016). Therefore, phases can co-precipitate sequentially during a single fracturing and fluid injection event. This may result in inclusions within their host crystal, despite both having formed during the same overall fracturing event. This phenomenon arises from small differences in how the phases respond to the transient and evolving geochemical and physical conditions. For example, galena can precipitate slightly earlier in hydrothermal veins than sphalerite due to the higher solubility of Zn in lower temperatures, compared to Pb (e.g. Barrett and Anderson 1988; Leach *et al.* 2001). Similarly, chalcopyrite often slightly predates both sphalerite and galena in the precipitation sequence due to the lower solubility of copper in decreasing fluid temperatures (Fig. 1e; Kamilli 1998). In mineralization processes that involve deterioration of Au-H<sub>2</sub>S metal-ligand complexes, sulfide and gold co-precipitation is also common with gold being captured within sulfides as inclusions (Huston and Large 1989; Liu *et al.* 2010). A further complication may be brought about by exsolution textures: an example of such a feature is ‘chalcopyrite disease,’ a term referring to the exsolution of sphalerite and chalcopyrite where the chalcopyrite typically manifests itself as intergrowths of varying morphologies within the

### Textural mapping and building a paragenetic interpretation

sphalerite (lamellae, blebs or vermicular; Fig. 1f; Eldridge *et al.* 1988; Bortnikov *et al.* 1991). These might be mistaken as inclusions but, on the other hand, the paragenetic implications of chalcopyrite disease are not conflicting with the interpretation of co-precipitation of the two sulfides, i.e. that they are coeval. Finally, phases precipitated early during a single fluid event can sometimes be fractured during the same event. For example, pyrite often precipitates from the solution faster than most other phases but it deforms relatively easily by both brittle and ductile means over a wide range of P-T conditions, including fracturing as a result of thermal expansion during (continued) depressurization (Cox *et al.* 1981; Liu *et al.* 2010). As a consequence, pyrite is often fractured during the ongoing event with possible deposition of other phases (such as gold or other sulfides) inside pyrite microfractures (Fig. 1g; Huston *et al.* 1992; Cook *et al.* 2013; Sahoo and Venkatesh 2015; Yang *et al.* 2016; Rogowitz *et al.* 2018; Li *et al.* 2020, 2022; Fougrouse *et al.* 2021). Either way, the implications of evolving fluid composition and physico-chemical conditions of precipitation to the paragenetic interpretation are profound: in all of the cases described above, the observed relationships imply a single fluid event/paragenetic stage, not two as conventional approaches to cross-cutting and inclusion relationships would suggest. On the other hand, specifically for gold it should be mentioned that gold can also be remobilized by a later fluid from the crystal lattice of pyrite precipitated in an earlier event, and redeposited in the pyrite fractures (Mills *et al.* 2015; Fougrouse *et al.* 2016; Lebrun *et al.* 2016; Hastie *et al.* 2020). A remobilization and local reprecipitation of gold in this way has been suggested by Hastie *et al.* (2020) as a mechanism to coarsen the gold grains in hydrothermal veins. A remobilization scenario, or an alternative scenario where gold in fractures has been brought in by a later fluid, would require two separate fluid events. When cross-cutting relationships are observed between pyrite and gold, more detailed microgeochemical investigations may, therefore, be needed of the pyrite to elucidate the most likely paragenetic position of the crack-hosted gold; the review of these is, however, outside the scope of this paper.

Another type of a texture belonging to this category is growth zoning. Growth zoning typically manifests itself as concentric zoning approximately tracing the euhedral crystal shape of the phase (Fig. 1h, i and k). In some cases, growth zoning arises from separate fluid events (Fig. 1h). In other cases, growth zoning can result from a single fluid event as a consequence of progressively changing or fluctuating composition of the fluid or magma from which the phase precipitates. This is a typical texture in e.g. quartz (Fig. 1i), pyrite (Fig. 1k) or in magmatic zircon. The interpretation and

implications of growth zoning are, therefore, intimately linked to understanding the general behaviour of the phase in question in the hydrothermal or magmatic system from which it precipitated.

Further challenges in interpreting inclusions and fractures arise also from the fact that thin sections are two-dimensional representations of three-dimensional rock volumes. The complications of making 3D interpretations of 2D thin sections have many implications to various applications within geosciences (e.g. Bandy 1940; Heilbronner and Bruhn 1998). In paragenetic analysis, the 3D connectivity of grains can be complex, resulting in erroneous interpretation of features. In particular, mutual crystal intergrowths may appear as if one phase is included in the other if the plane of the section is at right angles to the intergrowth direction, leading to the one phase being misidentified as inclusions. The best way to mitigate for this is to increase the number of observations (i.e. thin sections), including in other orientations, so that a more complete assessment of the three-dimensional textural aspects can be achieved.

Finally, it should be noted that material inherited from the wall rocks may in some cases be misinterpreted as inclusions representing an earlier hydrothermal fluid phase. Wall rock is often incorporated within hydrothermal veins as small breccia fragments. They are usually easy to identify as inherited fragments by their typically polyminerale compositions. However, in some cases individual crystals are entrained in veins that may be misinterpreted as having precipitated from earlier or coeval hydrothermal fluids. Correct interpretation of individual crystals becomes crucial, e.g. when identifying phases for geochronological analyses. An understanding of the chemical and mineralogical composition of the wall rock is essential to mitigate for this but, in addition, it is necessary to always perform a detailed textural analysis of the phases of interest.

### Alteration textures

Alteration is here defined as a phase in a rock being completely or partly replaced by another phase, due to a chemical reaction of the original phase with an ambient hydrous or carbonitic fluid phase (Schwartz 1959; Hemley and Jones 1964; Mathieu 2018). This is a slightly different definition from metamorphism where all reacting phases are typically solids or melts. Alteration textures are particularly common in rocks proximal to magmatic intrusions that contain a significant vapour phase, and within and around hydrothermal vein systems. In addition, in systems that involve several fracturing and fluid events (hydrothermal vein systems and many magmatic systems that involve several magmatic pulses), the fluid geochemistry can change between

successive fluid injection events. However, even without significant changes to the incoming fluid chemistry between the separate fluid events, the dynamic nature of the precipitation process in hydrothermal veins in particular means that the chemistry of the fluid in any single event can change during precipitation: therefore, especially those phases that precipitated late in the sequence can be in disequilibrium with the next incoming fluid pulse, making them susceptible to reactions with the new fluid. Whatever causes the disequilibrium between the solids and the fluid, the result is various alteration and other replacement reactions (Fig. 1j, k). These can be complete or partial, or only affect some phases and not the others, depending on whether or not that phase is in equilibrium with the fluid present. Identifying any alteration textures is crucial in constraining the paragenesis and can also inform on the nature and chemistry of the incoming fluid.

A specific form fluid-rock interaction and alteration is dissolution (Fig. 1j, k). Dissolution events typically manifest themselves as embayed, and often diffuse, crystal margins and/or intra-crystal boundaries, and as pores or patchy alteration textures within the original crystal. Dissolution can be followed by either reprecipitation of the dissolved phase or precipitation of a new phase - either proximally, at micron-scale (Rubatto *et al.* 2008; Hu *et al.* 2014; Zhu *et al.* 2021) or the dissolved material can move away and reprecipitate distally (Wangen and Munz 2004; Fougereuse *et al.* 2016; see also Hastie *et al.* 2020 and previous section re. gold remobilization-reprecipitation).

A note should be made here that, whilst sphalerite and chalcopyrite often co-precipitate or exsolve from a single fluid as discussed above, in certain conditions chalcopyrite has been suggested to represent a later, partial replacement of sphalerite by a solution enriched in Fe and Cu (e.g. Nagase and Kojima 1997). This would fundamentally change the interpreted number of fluid events, but a careful examination of the textural relationships and the morphologies of the crystals involved should, in most cases, be sufficient to mitigate this issue.

Alteration and dissolution textures are often relatively easy to identify, particularly if incomplete, although distinguishing zoning as a result of alteration (instead of primary growth) can be more challenging (Shore and Fowler 1996). Compositional zoning caused by alteration is perhaps most easily identified by the commonly diffuse or irregular or patchy nature of the zoning (Fig. 1j), whereas growth zoning tends to follow the crystal habit (Fig. 1i, k).

### *Crystal morphology*

Crystal morphology has historically had an important role in establishing paragenetic sequences, e.g.

coeval precipitation may be inferred from intergrowth textures (Newhouse 1927; Mookherjee 1964). In hydrothermal veins, euhedral crystal faces of particularly quartz are commonly interpreted as representing the first minerals to form in a paragenetic sequence because this morphology is facilitated by unimpeded growth into an open fracture space (Fig. 1i; Wilson 1994; Ahmed *et al.* 2009). Later minerals are, according to this approach, constrained by the pre-existing material and must grow around it, leading to concave faces and anhedral crystals. Whilst this is true in principle, in the context of hydrothermal veins with multiple fracturing events which will introduce new porosity (fractures and vugs) into the previously precipitated material, interpreting the euhedral grains as the first to form in the *entire* vein may be erroneous. Vugs, which are a common feature in hydrothermal veins, can be particularly difficult to interpret if filled with later phases, because can form at any stage during the repeated fracturing-sealing cycles of a typical hydrothermal vein system. In fact, as fractures normally become more connected over repeated fracturing episodes, the likelihood of vug formation increases in later mineralization stages due to the increased total volume of pore space (e.g. Tchalenko 1970).

Another complication related to crystal morphology arises from differences in the surface energies of phases. Some phases, such as garnet or pyrite, have very high surface energies and are capable of forming euhedral crystals whilst co-precipitating phases around them will show sub- to anhedral morphologies (e.g. Carstens 1986; Arrouvel and Eon 2019). A euhedral crystal shape is not, therefore, automatically an indication of it being precipitated earlier and, therefore, being paragenetically older than its surrounding phases.

### *Layering*

In stratiform ore deposits, the law of superposition (Steno 1669) has been used to establish stratigraphic sequences, most notably in colloform Mississippi Pb–Zn deposits, where sphalerite typically precipitates in layered sequences (Craig and Vaughan 1994). Provided that the unidirectional growth of the mineralized layers can be constrained and the grain size is suitable for the scale of observation, it is possible to interpret the paragenesis on the basis of layering. Craig and Vaughan (1994) described the use of banding as a paragenetic indicator as ‘sphalerite stratigraphy’; colour and/or composition are used to identify marker layers before tracing these over disparate localities in the same way that sedimentary horizons are correlated across basins (Fig. 1i; McLimans *et al.* 1980). These principles can, in theory, be applied to any form of banded ore deposit; for example, colloform or crustiform

## Textural mapping and building a paragenetic interpretation

textures in quartz are interpreted to represent rapid layered deposition in open-space (Bodnar *et al.* 1985; Fournier 1985). Therefore, the quartz bands closest to the vein wall(s) are oldest, with successive layers being deposited in the centre of the vein. However, care is needed as layered textures in hydrothermal veins do not typically form via simple sequential deposition. The cyclic fracturing-sealing processes and associated high pore fluid pressure gradients of most hydrothermal vein systems have been discussed in other contexts in this paper, but these processes also have implications to the layering in veins. Subsequent fracturing episodes can open up any part of a previously precipitated vein, including the vein-wall rock contact, and repeated crack-seal processes can result in veins with a 'laminated' or layered structure (Fig. 1b). Unless clear cross-cutting relationships can be observed, it can be impossible to visually determine precisely the order of the formation of the various sub-veins. Awareness of the process is, however, crucial especially when the individual layers are thicker than the area of a thin section, as this can influence both the sampling approach and interpretation of the observations.

### *Part 2: a workflow for developing a paragenetic interpretation*

The last part of this paper demonstrates a practical workflow, i.e. how the described theoretical and methodological considerations can be applied to developing a robust paragenetic interpretation using SEM, including documentation of the textural evidence. We have chosen a Au-Ag-Zn-Pb quartz vein at Glen Almond near Loch Tay, central Scotland, to illustrate the approach. We chose this vein as it shows evidence of a multi-generational precipitation history whilst also having a relatively simple mineralogy. Therefore, it is an excellent example to showcase the workflow for paragenetic interpretation via textural mapping.

A description of the general geological setting, which is very brief in this section where the focus is on workflow, is followed by detailed descriptions and documentation of the observations made during the textural mapping of the vein. The textural evidence is then used to build a paragenetic interpretation. The workflow case study finishes with a very brief demonstration on the main implications of the findings to the ore exploration in the area: an in-depth regional discussion is outside the scope of this paper.

As a general note, because paragenetic interpretation is based on evidence gathered via visual observations of textural relationships, a key aspect of the workflow is the inclusion of high-quality representative images, preferably with a supporting table to

summarize observations. We also recommend an approach to textural mapping that is not dissimilar from geological fieldwork in the sense that, in addition to high-quality digital images, a notebook should be used to record observations (including sketches of textural relationships) as they are made during both SEM and optical microscopy. A robust visual record of the textural relationships is essential as evidence for the construction of a paragenetic interpretation, which is typically illustrated by a paragenetic table where the interpreted temporal relationships of the different phases (i.e. distinct vein generations) are summarized.

### *Geological setting*

The case study area is located near Loch Tay, within the Grampian Terrane of Scotland (Fig. 2). It belongs to the Southern Highland Group of the Dalradian Supergroup comprised predominantly of Cambrian pelites and psammites with some layers of mafic lavas and tuffs, deposited onto the Laurentian passive margin (Stephenson *et al.* 2013; Tanner *et al.* 2013). The Grampian Terrane was pervasively deformed and metamorphosed during the Ordovician–Silurian Caledonian orogeny. The first Caledonian collisional event at *c.* 475–465 Ma was characterized by a ~NW–SE relative convergence with crustal thickening through thrust and nappe tectonics (e.g. Roberts and Treagus 1977; Baxter *et al.* 2002; Oliver *et al.* 2008; Chew and Strachan 2013; Tanner 2014a; Mark *et al.* 2020). The Grampian phase was followed by a period of uplift and unroofing until *c.* 430 Ma (e.g. Dempster 1985; Soper *et al.* 1999; Oliver 2001). The second phase of the Caledonian orogeny resulted in the final closure of the Iapetus Ocean and the docking of Avalonia against Laurentia between *c.* 435–410 Ma (e.g. Dewey and Mange 1999; Dallmeyer *et al.* 2001; Chew and Strachan 2013). This event did not result in further significant thickening of the crust in central Scotland and is mainly expressed as transpressional sinistral strike-slip movement along major transcurrent orogen-parallel faults (e.g. Dewey and Strachan 2003; Treagus 2003; Tanner 2014b). These structures which include the Loch Tay Fault in Figure 2 are widely recognized throughout the Grampian Terrane; they are probably long-lived structures but at least some of the fault activity has been dated to 416–395 Ma (Chew and Strachan 2013). Significant granitoid magmatism took place around the same time, from *c.* 425 Ma onwards (e.g. Jacques and Reavy 1994; Oliver *et al.* 2008; Neilson *et al.* 2009). Treagus *et al.* (1999) suggest that this emplacement of the late Silurian granites occurred in a transtensional setting, with a WSW–ENE directed regional extension. Certainly there was a transition from transpression to transtension near this time: by *c.* 410 Ma, Devonian Red

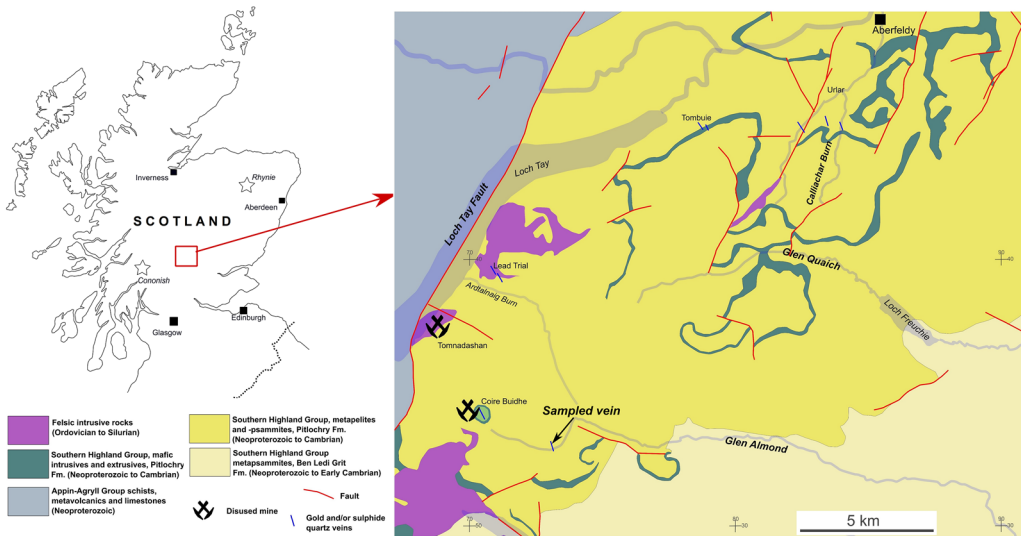


**Fig. 2.** Generalized geological map of the Loch Tay area, showing the locations and orientations of the known quartz-sulfide-gold veins, including the sampled Glen Almond vein. The inset outline of Scotland also shows the locations of the Cononish gold mine and Rhynie epithermal gold mineralization (see text).

Beds were being deposited into transtensional pull-apart basins across the Grampian Terrane (e.g. Dewey and Strachan 2003).

Gold occurs in the alluvial and glacial sediments throughout the Grampian Terrane of Scotland and Ireland (e.g. Chapman *et al.* 2000). The bedrock sources for these occurrences are mostly unknown but, in addition to the Glen Almond vein, various localities with gold-bearing quartz veins have been identified in the Grampian Terrane in Scotland (Cononish gold mine in Tyndrum; Calliachar-Urlar and Tombuie areas near Loch Tay; and Rhynie in NE Aberdeenshire; e.g. Patrick *et al.* 1988; Rice *et al.* 1995; Ixer *et al.* 1997; Corkhill *et al.* 2010; Spence-Jones *et al.* 2018). In addition, several gold-bearing vein systems are known in Ireland and Northern Ireland (notably Curraghinalt, Cavanacaw and Croagh Patrick; Wilkinson and Johnston 1996; Wilkinson *et al.* 1999; Parnell *et al.* 2000; Rice *et al.* 2016; Shaw *et al.* 2022). Which phase of the Caledonian-Adian tectonism resulted in the formation of the veining and the gold mineralization in the Grampian Terrane of Scotland is partly an open question as few of the vein systems have been directly dated, but available age data implies that at least Cononish and Rhynie were deposited at *c.* 410 Ma, i.e. at the late stages of the Scandian phase or during the transition from transpression to extension (Treagus *et al.* 1999; Mark *et al.* 2011).

In the Loch Tay area, there are several sulfide-bearing quartz( $\pm$ carbonate) veins, some of which may be economical: in particular, a gold-bearing

vein array has been identified by Green Glen Minerals Ltd (formerly Erris Gold Resources Ltd.) at Lead Trial near Ardtalnaig in 2020–21. Little published information exists of the known Loch Tay vein system. Some observations of the mineralogy and the cross-cutting relationships using TLM and RLM have been published for the Calliachar-Urlar vein in Ixer *et al.* (1997) and for Coire Buidhe in Patrick (1984), and Corkhill *et al.* (2010) describe mineralization in the Tombuie veins. None of the papers provide a complete paragenetic interpretation. All the veins are subvertical with fairly consistent NNW–SSE strikes.

The Glen Almond vein was identified by the authors in 2019. The vein is part of the wider Loch Tay vein system, the detailed characterization of which is a part of a larger research project by the authors (Chapman *et al.* 2023). The vein strikes NNW–SSE and cross-cuts a layered package consisting of Dalradian metasedimentary schists. Its mineralogy is predominantly quartz with the main sulfides consisting of galena, sphalerite and pyrite, with some chalcopyrite (Fig. 3). Late carbonate-bearing fractures cut the vein and its host schists. The outcrop of the vein is small, only slightly over 1 m long and the exposed vein is up to *c.* 20 cm in thickness. The steeply dipping vein margins are sharp with the host rock. The vein shows a variety of textures but it is mostly massive with occasional vugs with euhedral crystals (Fig. 3 inset) indicative of significant dilation and high pore fluid pressure gradients during at least some stage(s) of fracturing.

## Textural mapping and building a paragenetic interpretation

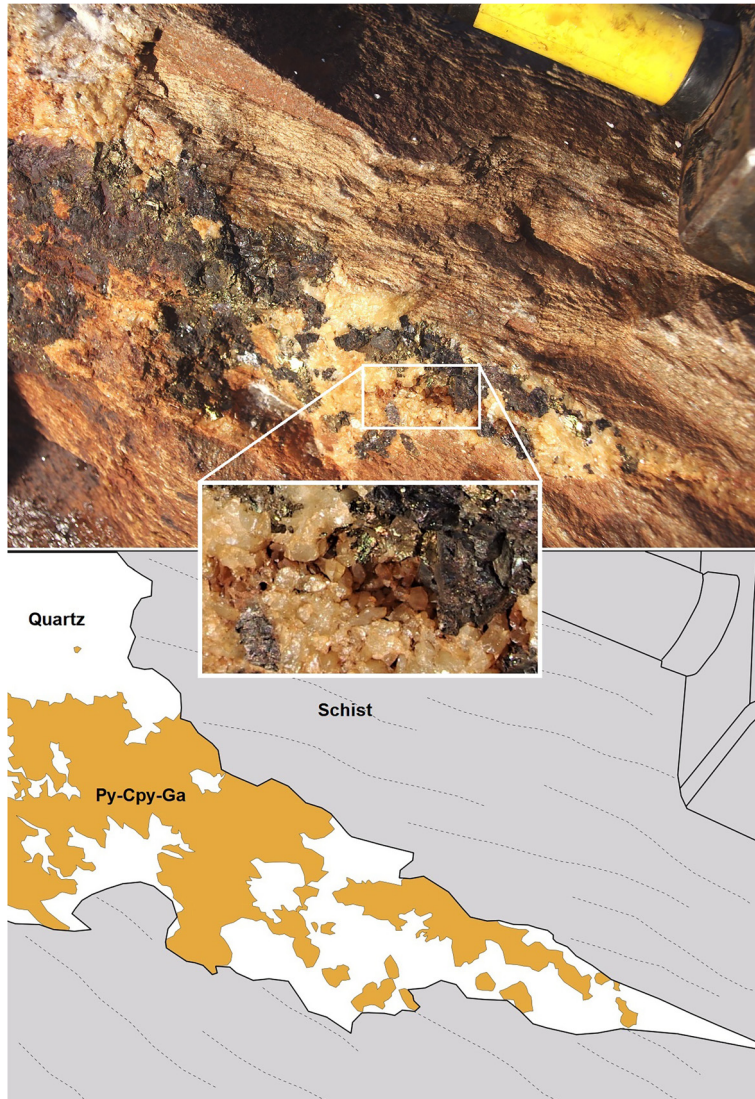


**Fig. 3.** Photograph and its line drawing of a sulfide-rich (pyrite-chalcopyrite-galena) part of the Glen Almond vein at the sampling locality. The vein texture is mostly massive but there are some vugs outlined by sub- to euhedral crystal faces of quartz and sulfides (inset). Note that the outcrop surface is oblique to the vein strike, resulting in vein margins that appear irregular, whereas the NNW–SSE striking vein in reality cuts the host rock sharply.

### *Description of the textural relationships*

This section highlights how observations made during the textural mapping can be documented and communicated. It is important that observations are presented in a systematic, comprehensive and representative manner, and clearly separated from interpretations.

Five polished blocks (RC1-5) and one thin section (AVRE) from the Glen Almond vein were

analysed with an SEM. The entire thin section was scanned with a TLM scanner before analysis to aid navigation; and overview SEM scans of all polished blocks were also prepared for the same reason. [Table 1](#) and [Figure 4](#) document the SEM observations that are considered representative for the analysed samples and used as evidence for the final paragenetic interpretation. We briefly summarize these observations below. The observations are described with letter nominations, instead of

**Table 1.** Summary of the observations made during textural mapping, with references to representative SEM images (Fig. 4)

Mineral	Thin section (s) ID	A	B	C	D	E
<b>Quartz</b>	AVRE	Early qtz stage, often zoned. Brecciated by all later phases. <a href="#">Figure 4b.</a>	QtzB + C filled fractures brecciating the early zoned qtz, brecciated by DolD. QtzB/QtzC indistinguishable in CL <a href="#">Figure 4b.</a>			Hairline fractures cutting all previous generations and sulfides. <a href="#">Figure 4c.</a>
<b>Pyrite</b>	RC2, RC5 (4)		PyB: BSE-darker, No As (contrary to PyC). Some <5 um Sph, Ga, Cpy and Au inclusions. <a href="#">Figure 4a, d-f.</a>	PyC: BSE-lighter than PyB, c. 1.5 wt% As. As rims around/in fractures within PyB, or as individual crystals. Small Ga, Cpy along interfaces btw PyB and PyC. Co-precipitates with Au, sph and cpy (Au often in fractures in the py). <a href="#">Figure 4a, b and d-g.</a>		
<b>Chalcopyrite</b>	RC5(4)  RC1, RC2, RC3, RC4 (5)		Small blebs of cpy within PyB. <a href="#">Figure 4e.</a>	CpyC: Fractured, co-precipitates with late PyC, AuC, SphC, Cross-cut by fractures with QtzE and GaE. Also as small inclusions within SphC. <a href="#">Figures 1f, 4g and h.</a>		
<b>Galena</b>	RC2, RC5(4)		Early GaB:, <5 um, co-precipitating with Au in the no-As darker py. <a href="#">Figure 4b.</a>	GaC (or late GaB): very small (<10 um) blobby grains only seen along interfaces between PyB and PyC. <a href="#">Figure 4b.</a>		

	RC1			GaE: large >>100 um crystals with visible cleavage and in hairline fractures. Intergrown with SphE. Cross-cuts all earlier phases. <a href="#">Figure 4d</a> .
<b>Sphalerite</b>	RC1, RC2, RC5(4)	SphB: <5 um inclusions of sph within early PyB. <a href="#">Figure 4b</a> .	SphC: grains >100 um, co-precipitates with CpyC, AuC and PyC although the Au and Cpy often brecciate the Sph. Occasional <5 um cpy exsolution blebs. Cross-cut by fractures with QtzE and GaE. <a href="#">Figure 4c</a> .	SphE: very large >>100 um crystals intergrown with GaE. Cross-cuts all earlier phases. <a href="#">Figure 4d</a> .
<b>Gold</b>	RC2, RC4 (5)	AuB: Blebby Au inclusions within PyB (<5 um), co-precipitates with Ga. Lower Ag content ~25% than AuC. <a href="#">Figure 4b</a> .	AuC: in cracks (mostly py and sph) with co-precipitating cpy and qtz. Higher Ag content ~35% than AuB and coarser (up to ~100 um). <a href="#">Figure 4b, c</a> .	
<b>Carbonate</b>	AVRE AVRE, RC1	AuC or AuB: circular gold grains <5 um in QtzB + C.		DoID: cross-cuts earlier phases; cross-cut by late sulfides and hairline fractures. Crystals up to >100 um. <a href="#">Figure 4d</a> .

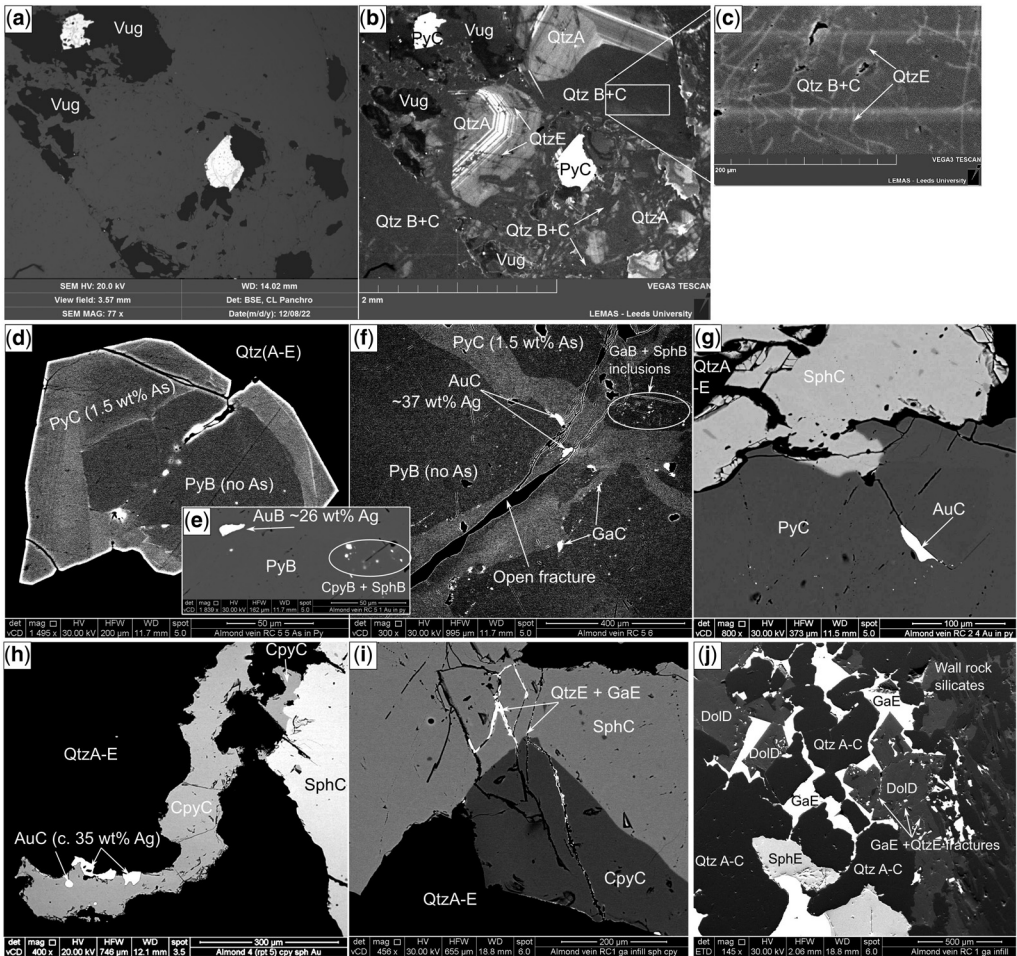


**Fig. 4.** SEM and BSE photographs of representative vein textures illustrating the relationships described in Table 1. (a–c) The quartz generations in the Almond Vein and association of sulfides within them. (a) BSE image: the vugs and the pyrite grains (light grey) are clearly imaged, but the internal textures of the quartz (dark grey) cannot be resolved. The pyrite is affected by supergene oxidation, expressed by the medium-grey dots and fractures within the pyrite grains; (b) and (c) CL imaging enables observing three different types of quartz in the sample. The early, typically zoned, quartz A is brecciated by a voluminous, fairly CL-homogeneous quartz that, based on wider observations, must consist of at least two generations (B + C; see text). The homogeneous quartz B + C are associated with most of the sulfides (here pyrite). Thin hairline fractures (QtzE) cut all previous generations: (c) shows a high-contrast CL detail of the more homogeneous QtzB + C, showing the hairline fracturing; (d–g) High-contrast BSE images of various pyrite stages. The darker pyrite PyB is enveloped (Fig. 4d) or fractured (Fig. 4f) by lighter-grey PyC. PyC also grows as individual grains with other sulfides (Fig. 4g). PyB can be distinguished from PyC via inclusion suites and As content: PyB is As-free and contains abundant micron-scale inclusions of GaB, CpyB and SphB (Fig. 4e, f) as well as gold with ~26 wt% Ag (AuB; Fig. 4e). PyC, in contrast, is typically fairly inclusion-free and consistently contains *c.* 1.5 wt% As. Galena (GaC) is commonly precipitated at the interface between PyB and PyC (Fig. 4f) but is only very rarely found as inclusions within PyC. PyC contains gold in fractures, the gold being richer in Ag and coarser than AuB (Fig. 4f, g). The observation that AuC is often found in fractures within PyC associated with other sulfides indicates that this stage involved a common scenario of continuum precipitation of the sulfides and gold, with the pyrite precipitating early in the sequence (see text). (h) and (i) BSE images showing the relationships between stage C sphalerite, chalcopyrite and gold, and a later, stage E galena and quartz. In both images, AuC, SphC and CpyC show co-precipitation textures (intergrown crystal faces; see also Fig. 4g). These phases are cross-cut by quartz and galena-bearing fractures (QtzE and GaE in Fig. 4i). CpyC is also present as small, medium-grey, rounded inclusions within SphC in (g) (chalcopyrite disease; see also Fig. 1f). (j) A BSE image showing the relationships of the last two precipitation stages. A Mg-rich carbonate (DoID) brecciates the earlier phases but is in turn brecciated by the voluminous, late sphalerite and galena (SphE and GaE), and quartz (QtzE).

### Textural mapping and building a paragenetic interpretation

numbers, to clearly distinguish them from the interpretations presented later in this section.

*Quartz* is in CL seen to show typically zoned crystals (QtzA), pervasively brecciated by CL-homogeneous quartz filling the fractures (Table 1, Fig. 4b). It is not possible to distinguish multiple quartz generations within this CL-homogeneous quartz but for consistency, we have termed this quartz QtzB + C because it is associated with both sulfides B and C (as described below). QtzA-C are brecciated by fractures filled with DolD and GaE, SphE and QtzE (Fig. 4c, j).

*Pyrite* is associated with QtzB + C (Fig. 4a, b) and shows complex textural relationships with other sulfides and gold. There are two pyrite types in the samples: a slightly BSE-darker pyrite (PyB) and another, BSE-lighter pyrite (PyC) that precipitates either around or in the fractures of PyB, or as individual, up to mm-scale grains (Fig. 4d–g). PyB has micron-scale rounded inclusions of gold, galena, sphalerite and chalcopyrite (AuB, GaB, SphB, CpyB; Fig. 4e, f; Table 1). EDX semi-quantitative analysis shows that PyB contains no arsenic, whereas PyC contains small amounts of As (c. 1.5 wt%). The interface of PyB and PyC commonly contain small grains of galena (GaC) and sometimes chalcopyrite (Fig. 4f), but most of PyC is inclusion-free and the sulfides and gold associated with PyC precipitated together with, or slightly later than, the pyrite (Fig. 4c).

*Chalcopyrite and sphalerite.* There are two types of chalcopyrite and three types of sphalerite in the samples. Some of the chalcopyrite and sphalerite are seen as micron-scale inclusions within PyB (Fig. 4e); chalcopyrite is also very occasionally seen along the PyB-PyC interfaces. The second, most voluminous cpy and sph occur as up to mm-scale grains co-precipitating with each other, PyC pyrite and gold (CpyC and SphC; Fig. 4g–i). In addition, micron-scale CpyC inclusions are common within SphC (chalcopyrite disease; Figs 1f and 4g). A third sphalerite type (SphE) co-precipitates with coarse galena and quartz (GaE and QtzE) that are seen to cross-cut all other phases (Fig. 4j).

*Galena* occurs as two types: as micron-scale inclusions within PyB and along PyB-PyC interfaces (Fig. 4d, f). Contrary to pyrite, sphalerite and chalcopyrite, however, no galena seems to have precipitated during the main stage C. The second galena type to precipitate is associated with the late hairline fractures and coarse SphE cross-cutting all previous phases, including stage D carbonates (Fig. 4i, j).

*Carbonates*, mostly Mg dolomite, occur as one type only: DolD precipitated as up to mm-scale, sub-to euhedral crystals in fractures cross-cutting stage A-C crystals (Fig. 4j). DolD is in turn fractured by GaE, SphE and QtzE.

*Gold* precipitated as three types. The first type occurs as micron-scale inclusions within PyB (Fig. 4e). Semi-quantitative EDX analysis shows that this gold consistently contains c. 25–26 wt% Ag. The second gold type is associated with stage C sulfides (Fig. 4f, g). This gold is distinguished from AuB by its coarser grain size and higher Ag content (35–37 wt% Ag). It occurs together with CpyC and within cracks of SphC and PyC. The third type of gold has been identified as micron-scale inclusions within QtzB + C: we have not been able to establish further textural relationships or Ag content for this gold type.

### Paragenetic interpretation

This section demonstrates how the evidence from the textural mapping is used to arrive at an interpretation of the paragenesis. The paragenetic interpretation of the Glen Almond vein is based mostly on cross-cutting relationships and inclusions across several samples (thin sections and polished blocks). An important general note is that a robust paragenetic interpretation necessitates a careful inspection of several thin sections and polished blocks: the case study clearly illustrates that the complete set of relationships are not usually observable in a single sample, even for a relatively small vein such as the Glen Almond vein.

Using the mapped textural relationships described above, we have interpreted the paragenesis and the evolution of the mineralization in the Glen Almond vein, presented as a paragenetic table in Figure 5. Quartz is the dominant gangue mineral in the vein as it is observed with all other phases apart from stage D carbonates. The initial fracturing event (Stage 1) precipitated only quartz, with typically zoned grains (QtzA). The next events (Stage 2 and Stage 3) are evidenced by QtzA being fractured by the CL-homogeneous quartz (QtzB + C) and its associated sulfides and gold. Stage 2 and Stage 3 seem to form a precipitation continuum: the sulfides and gold show a textural and geochemical evolution but the quartz associated with B and C sulfides is CL-homogeneous (i.e. geochemically indistinguishable), implying that the underlying fluid composition did not change significantly. We have, however, separated Stage 2 and Stage 3 here because certain clear mineralogical variations can be observed which we interpret to indicate repeated (at least two) fluid pulses rather than a chemical evolution of a fluid injected in a single, protracted event: During Stage 2, the volume of precipitated sulfides and gold was small, the pyrite contains no arsenic and the gold has a lower silver content than the later, Stage 3 gold. SphB, CpyB and GaB inclusions within PyB have rounded, poorly defined edges and typically occur in clusters: such morphologies are

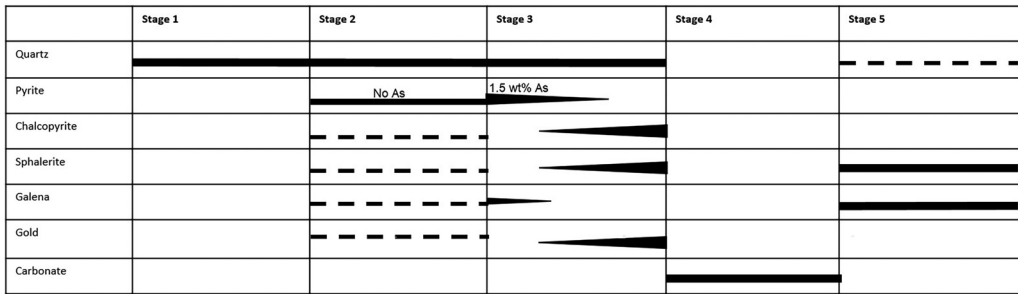


**Fig. 5.** Paragenetic interpretation of the Glen Almond vein, based on the mapped textural relationships. The thickness and continuity of the line indicates the relative volumes between stages (thicker line = more/very voluminous; thinner line = less voluminous; stippled line = rare/very small volume). A tapered line indicates that the precipitated mineral is phased in or out during the precipitation stage.

typical of co-precipitation (e.g. Imai 1999). In contrast to the other sulfides, galena is absent in Stage 3, apart from having precipitated at the interface between PyB and PyC as a very early phase of Stage 3. Sphalerite and chalcopyrite, with Ag-richer gold and some pyrite containing a small amount of As, dominate the late Stage 3 precipitation, with all sulfides and the gold being much more voluminous and coarser-grained (typically mm-scale sulfides) than in Stage 2.

A separate, carbonate-rich fluid was injected into fractures within the vein during Stage 4. No conclusive evidence of coeval quartz precipitation at this stage was found. The last fluid injection event seen in the samples is Stage 5 where all previous phases are brecciated by fractures carrying coarse galena and sphalerite: some quartz is present particularly in hairline fractures but the precipitated phases are dominated by the sulfides. No gold associated with this stage has been identified in the Glen Almond vein.

## Discussion

This last section of the case study briefly demonstrates how the textural evidence and the paragenetic interpretation can be put into the context of the Loch Tay metallogeny and ores exploration. A comprehensive discussion is beyond the scope of this paper so we focus on the immediate implications of our paragenetic interpretation.

Our study is the first complete paragenetic interpretation of any of the veins in the Loch Tay area. Despite the similar main phase assemblages in the veins across the area and very consistent strike orientations of all veins, there are some clear mineralogical differences between the Glen Almond vein and the other Loch Tay veins, based on published literature. At Calliachar, nickeliferous minerals,

arsenopyrite and pyrrhotite are present (Iyer *et al.* 1997) and alluvial gold grains collected in Calliachar Burn contain inclusions of various cobalt, nickel and arsenic phases (Chapman *et al.* 2023). The Coire Buidhe veins contain Pb-Bi-Ag sulfosalts, arsenopyrite and pyrrhotite, but also siderite and native bismuth (Patrick 1984). All of these minerals seem to be absent in the sampled Glen Almond vein. The mineralogical differences are tentatively explained by a late re-opening of the larger veins and injection of a new fluid, the source and composition of which may vary between areas. In other words, the small size of the Glen Almond vein may indicate a lack of significant re-opening/reactivation, as opposed to the much bigger (up to *c.* 2 m thick) veins at Calliachar, Coire Buidhe and Lead Trial which all show phases that are absent at Glen Almond. Alternatively, the mineralogical differences might reflect local variations in lithology, i.e. different styles of fluid-wall rock interaction. Different fluid sources for each vein locality cannot be ruled out either, although this seems unlikely with the view of the similarities in the main sulfide assemblages and the very consistent vein strikes across the area.

Our paragenetic interpretation implies a common fluid source for Stages 2 and 3, based on the broad mineralogical similarities and the similarity of quartz B and C in CL. However, the evidence from the sulfides strongly suggest that this fluid was injected into the vein during at least two separate events: two gold (and sulfide) types precipitated in the Glen Almond vein during Stages 2 and 3. The first gold generation (Stage 2; AuB) is found as inclusions within pyrite PyB with other sulfides, whilst Stage 3 gold (AuC) occupies fractures affecting Stage 2 phases and Stage 3 pyrite. The AuB alloy has systematically a lower Ag content than the coarser AuC, although it should be noted that the difference in the Ag content is not large enough to be used as a definite genetic discriminator: the Ag content of gold alloy can

## Textural mapping and building a paragenetic interpretation

evolve during a single fluid event (Gammons and Williams-Jones 1997) and a continuum of Ag contents in gold grains is often found in studies involving large gold grain datasets (Chapman *et al.* 2021). The textural and compositional characteristics described, including the observed differences in the associated sulfides suggest, however, that AuB and AuC probably precipitated at different times, from different fluid events. This interpretation, along with the more general evidence of a multi-stage fracturing and phase precipitation history for the Glen Almond vein, shows that the vein formed via cycles of fracturing, fluid injection, and sealing via mineral precipitation.

The paragenesis has some implications to exploration and regional metallogeny. The metallic mineralization shows some commonalities across the Loch Tay area veins, with all veins containing some gold, pyrite, galena and chalcopyrite, although sphalerite is less common. This implies that the metallic mineralization in the area is not conditional to more local, vein-specific fluid chemistries or local fluid-rock interactions (although these may have played a role in some of the variation observed in the vein mineralogies). There seems to be no direct association between galena and (AuC) gold precipitation at Glen Almond: although both galena and gold are present as small inclusions in Stage 2 pyrite, the later more voluminous and coarser Stage 3 gold seems to be unrelated to galena precipitation. Whether this holds true for the other Loch Tay veins is unclear and further investigation is required, but if this is a generic feature it has implications for interpreting regional soil geochemical data. In particular, the lead content of soil samples is not necessarily the most reliable proxy for gold mineralization whilst zinc or copper may be more directly associated with gold. Furthermore, there seems to be an absence of arsenopyrite in the Glen Almond vein, although a small amount of As was found in Stage 3 pyrite. Therefore, As may also be an unreliable proxy for gold in soil geochemical exploration in the area although, again, the general applicability of this observation remains unknown until detailed paragenetic interpretations are available for the other Loch Tay veins.

## Conclusion

In this paper, we have established that textural mapping and interpretation of paragenesis is an exercise that can be undertaken across the spectrum of geosciences, mainly with the purpose of contextualizing phases that may be subject to further analysis. Paragenetic interpretation is particularly complex in the analysis of hydrothermal vein systems. Over the years, paragenetic studies have gradually become

more sophisticated, in terms of both the analytical equipment typically deployed and the application of the results.

We have described the theoretical considerations and approaches for textural mapping and paragenetic interpretation, and demonstrated a practical workflow applying these principles, via a case study developing a paragenetic interpretation for the gold-sulfide-bearing Glen Almond vein near Loch Tay, Scotland. The Glen Almond case study particularly emphasizes the importance of textural mapping and paragenetic interpretation to ore geology, in which the results may have ramifications for understanding regional metallogeny and for exploration. We have approached the paper and the workflow case study from the viewpoint of ore geology and hydrothermal veins, in which paragenetic interpretations are commonly used, but the principles and the workflow outlined in this paper are equally applicable to any discipline and route of investigation that necessitates a robust understanding of the spatial and temporal relationships of the phases in a rock.

**Acknowledgements** SW and LS are supported by the Leeds-York-Hull National Environment Research Council (NERC) Panorama Doctoral Training Partnership (DTP). We are grateful to Green Glen Minerals for their help and support, and to Richard Walshaw and Harri Wyn Williams for the help with sample preparation and SEM analyses. Tom Blenkinsop and Anne-Sylvie André-Mayer are gratefully acknowledged for their helpful reviews of the manuscript.

**Competing interests** The authors declare that they have no known competing financial interests or personal relationships that could have appeared to influence the work reported in this paper.

**Author contributions** SW: conceptualization (equal), data curation (equal), formal analysis (equal), visualization (supporting), writing – original draft (equal), writing – review & editing (supporting); TT: conceptualization (equal), data curation (equal), formal analysis (supporting), supervision (lead), visualization (lead), writing – original draft (equal), writing – review & editing (lead); RC: conceptualization (supporting), data curation (supporting), formal analysis (equal), visualization (supporting), writing – original draft (supporting), writing – review & editing (supporting); LS: data curation (supporting), formal analysis (equal), writing – review & editing (supporting).

**Funding** Lucia Savastano and Shane Webb thank Natural Environment Research Council for financial support.

**Data availability** All data generated or analysed during this study are included in this published article or held with authors and are available on request.

## References

- Ahmed, A., Arai, S. and Ikenne, M. 2009. Mineralogy and Paragenesis of the Co-Ni Arsenide Ores of Bou Azzer, Anti-Atlas, Morocco. *Economic Geology*, **104**, 249–266, <https://doi.org/10.2113/gsecongeo.104.2.249>
- Alford, L., Gysi, A., Hurtig, N., Monecke, T. and Pfaff, K. 2020. Porphyry-related polymetallic Au-Ag vein deposit in the Central City district, Colorado: mineral paragenesis and pyrite trace element chemistry. *Ore Geology Reviews*, **119**, 103295, <https://doi.org/10.1016/j.oregeorev.2019.103295>
- Andersen, J., Stickland, R., Rollinson, G. and Shail, R. 2016. Indium mineralisation in SW England: host parageneses and mineralogical relations. *Ore Geology Reviews*, **78**, 213–238, <https://doi.org/10.1016/j.oregeorev.2016.02.019>
- Arrouvel, C. and Eon, J.-G. 2019. Understanding the surfaces and crystal growth of pyrite FeS<sub>2</sub>. *Materials Research*, **22**, <https://doi.org/10.1590/1980-5373-MR-2017-1140>
- Babo, J., Spandler, C., Oliver, N., Brown, M., Rubenach, M. and Creaser, R. 2017. The High-Grade Mo-Re Merlin Deposit, Cloncurry District, Australia: paragenesis and geochronology of hydrothermal alteration and ore formation. *Economic Geology*, **112**, 397–422, <https://doi.org/10.2113/econgeo.112.2.397>
- Bandy, M. 1940. A theory of mineral sequence in hypogene ore deposits. *Economic Geology*, **35**, 359–381, <https://doi.org/10.2113/gsecongeo.35.3.359>
- Barrett, T.J. and Anderson, G.M. 1988. The solubility of sphalerite and galena in 1–5 m NaCl solutions to 300° C. *Geochimica Cosmochimica Acta*, **52**, 813–820, [https://doi.org/10.1016/0016-7037\(88\)90353-5](https://doi.org/10.1016/0016-7037(88)90353-5)
- Baxter, F.B., Ague, J.J. and Depaolo, D.J. 2002. Prograde temperature–time evolution in the Barrovian type-locality constrained by Sm/Nd garnet ages from Glen Clova, Scotland. *Journal of the Geological Society, London*, **159**, 71–82, <https://doi.org/10.1144/0016-76901013>
- Bortnikov, N., Genkin, A., Dobrovolskaya, M., Muravitskaya, G. and Filimonova, A. 1991. The nature of chalcopyrite inclusions in sphalerite; exsolution, coprecipitation, or ‘disease’?. *Economic Geology*, **86**, 1070–1082, <https://doi.org/10.2113/gsecongeo.86.5.1070>
- Bodnar, R., Reynolds, T. and Kuehn, C. 1985. Fluid-inclusion systematics in epithermal systems. In: Berger, B.R. and Bethke, P.M. (eds) *Geology and Geochemistry of Epithermal Systems*. Reviews in Economic Geology, 73–97, <https://doi.org/10.5382/Rev.02.05>
- Bowes, D.R. 1989. *The Encyclopedia of Igneous and Metamorphic Petrology*. Van Nostrand Reinhold, New York.
- Brammhall, A., Leech, J. and Bannister, F. 1937. The paragenesis of Cookeite and hydromuscovite associated with gold at Ogofau, Carmarthenshire. *Mineralogical Magazine and Journal of the Mineralogical Society*, **24**, 507–520, <https://doi.org/10.1180/minmag.1937.024.157.01>
- Breithaupt, A. 1849. *Die Paragenesis der Mineralien*, 1st edn. Freiburg im Breisgau.
- Butler, R.W.H. and Torvela, T. 2018. The competition between rates of deformation and solidification in syn-kinematic granitic intrusions: resolving the pegmatite paradox. *Journal of Structural Geology*, **117**, 1–13, <https://doi.org/10.1016/j.jsg.2018.08.013>
- Carstens, H. 1986. Displacive Growth of Authigenic Pyrite. *Journal of Sedimentary Research*, **56**, 252–257.
- Chapman, R., Banks, D. *et al.* 2021. Chemical and physical heterogeneity within native gold: implications for the design of gold particle studies. *Mineralium Deposita*, **56**, 1563–1588, <https://doi.org/10.1007/s00126-020-01036-x>
- Chapman, R.J., Leake, R.C., Moles, N.R., Earls, G., Cooper, C., Harrington, K. and Berzins, R. 2000. The Application of microchemical analysis of alluvial gold grains to the understanding of complex local and regional gold mineralization: a case study in the Irish and Scottish Caledonides. *Economic Geology*, **95**, 1753–1773, <https://doi.org/10.2113/gsecongeo.95.8.1753>
- Chapman, R.J., Torvela, T. and Savastano, L. 2023. Insights into regional metallogeny from detailed compositional studies of alluvial gold: an example from the Loch Tay area, central Scotland. *Minerals*, **13**, <https://doi.org/10.3390/min13020140>
- Chew, D. and Strachan, R. 2013. The Laurentian Caledonides of Scotland and Ireland. *Geological Society, London, Special Publications*, **390**, 45–91, <https://doi.org/10.1144/SP390.16>
- Combes, E., Eglinger, A., André-Mayer, A.-S., Teitler, Y., Heuret, A., Gilbert, P. and Béziat, D. 2021. Polyphase Gold Mineralization at the Yaou Deposit, French Guiana. *Geological Society, London, Special Publications*, **516**, 177–210, <https://doi.org/10.1144/SP516-2020-29>
- Cook, N., Ciobanu, C., Meria, D., Silcock, D. and Wade, B. 2013. Arsenopyrite-pyrite association in an Orogenic Gold Ore: tracing mineralization history from textures and trace elements. *Economic Geology*, **108**, 1273–1283, <https://doi.org/10.2113/econgeo.108.6.1273>
- Corkhill, C., Ixer, R., Mason, J., Irving, D. and Pattrick, R. 2010. Polymetallic auriferous vein mineralization near Loch Tay, Perthshire, Scotland. *Scottish Journal of Geology*, **46**, 23–30, <https://doi.org/10.1144/0036-9276/01-378>
- Cox, S., Etheridge, M. and Hobbs, B. 1981. The experimental ductile deformation of polycrystalline and single crystal pyrite. *Economic Geology*, **76**, 2105–2117, <https://doi.org/10.2113/gsecongeo.76.8.2105>
- Craig, J. and Vaughan, D. 1994. *Ore Microscopy and Ore Petrography*, 2nd edn. Wiley & Sons, New York.
- Dallmeyer, R.D., Strachan, R.A., Rogers, G., Watt, G.R. and Friend, C.R.L. 2001. Dating deformation and cooling in the Caledonian thrust nappes of north Sutherland, Scotland: insights from 40Ar/39Ar and Rb–Sr chronology. *Journal of the Geological Society, London*, **158**, 501–512, <https://doi.org/10.1144/jgs.158.3.501>
- Davidson, M. and Lofgren, G. 1991. Photomicrography in the Geological Sciences. *Journal of Geological Education*, **39**, 403–418, <https://doi.org/10.5408/0022-1368-39.5.403>
- deMelo, G., Monteiro, L. *et al.* 2016. Temporal evolution of the giant Salobo IOCG deposit, Carajás Province (Brazil): constraints from paragenesis of hydrothermal alteration and U–Pb geochronology. *Mineralium Deposita*, **52**, 709–732, <https://doi.org/10.1007/s00126-016-0693-5>

## Textural mapping and building a paragenetic interpretation

- Dempster, T. 1985. Uplift patterns and orogenic evolution in the Scottish Dalradian. *Journal of the Geological Society, London*, **142**, 111–128, <https://doi.org/10.1144/gsjgs.142.1.0111>
- Dewaele, S., Muchez, P., Heijlen, W., Boutwood, A., Lemmon, T. and Tyler, R. 2006. Reconstruction of the hydrothermal history of the Cu–Ag vein-type mineralisation at Dikulushi, Kundelungu Foreland, Katanga, D.R. Congo. *Journal of Geochemical Exploration*, **89**, 376–379, <https://doi.org/10.1016/j.gexplo.2005.11.010>
- Dewey, J.F. and Mange, M. 1999. Petrography of Ordovician and Silurian sediments in the western Irish Caledonides: tracers of a short-lived Ordovician continent – arc collision orogeny and the evolution of the Laurentian Appalachian-Caledonian margin. *Geological Society, London, Special Publications*, **164**, 55–107, <https://doi.org/10.1144/GSL.SP.1999.164.01.05>
- Dewey, J.F. and Strachan, R.A. 2003. Changing Silurian–Devonian relative plate motion in the Caledonides; sinistral transpression to sinistral transtension. *Journal of the Geological Society, London*, **160**, 219–229, <https://doi.org/10.1144/0016-764902-085>
- Dominy, S.C., Stephenson, P.R. and Annels, A.E. 2001. Classification and Reporting of Mineral Resources for High-Nugget Effect Gold Vein Deposits. *Exploration and Mining Geology*, **10**, 215–233, <https://doi.org/10.2113/0100215>
- Eldridge, C., Bourcier, W., Ohmoto, H. and Barnes, H. 1988. Hydrothermal inoculation and incubation of the chalcopyrite disease in sphalerite. *Economic Geology*, **83**, 978–989, <https://doi.org/10.2113/gsecongeo.83.5.978>
- Engel, A., Clayton, R. and Epstein, S. 1958. Variations in Isotopic Composition of Oxygen and Carbon in Leadville Limestone (Mississippian, Colorado) and in its Hydrothermal and Metamorphic Phases. *The Journal of Geology*, **66**, 374–393, <https://doi.org/10.1086/626524>
- Fan, G.-H., Li, J.-W., Deng, X.-D., Gao, W.-S. and Li, S.-Y. 2021. Age and Origin of the Dongping Au-Te Deposit in the North China Craton Revisited: evidence from Paragenesis, Geochemistry, and In Situ U-Pb Geochronology of Garnet. *Economic Geology*, **116**, 963–985, <https://doi.org/10.5382/econgeo.4810>
- Finlayson, A. 1910. The paragenesis of British ores. *Economic Geology*, **5**, 719–728, <https://doi.org/10.2113/gsecongeo.5.8.719>
- Fougerouse, D., Micklethwaite, S. *et al.* 2016. Gold remobilisation and formation of high grade ore shoots driven by dissolution-precipitation replacement and Ni substitution into auriferous arsenopyrite. *Geochimica et Cosmochimica Acta*, **178**, 143–159, <https://doi.org/10.1016/j.gca.2016.01.040>
- Fougerouse, D., Reddy, S. *et al.* 2021. A new kind of invisible gold in pyrite hosted in deformation-related dislocations. *Geology*, **49**, 1225–1229, <https://doi.org/10.1130/G49028.1>
- Fournier, R. 1985. The Behavior of Silica in Hydrothermal Solutions. In: Berger, B.R. and Bethke, P.M. (eds) *Geology and Geochemistry of Epithermal Systems*. Reviews in Economic Geology, 45–61.
- Frelinger, S.N., Ledvina, M.D., Kyle, J.R. and Zhao, D. 2015. Scanning electron microscopy cathodoluminescence of quartz: principles, techniques and applications in ore geology. *Ore Geology Reviews*, **65**, 840–852, <https://doi.org/10.1016/j.oregeorev.2014.10.008>
- Fulignati, P. 2020. Clay minerals in hydrothermal systems. *Minerals*, **10**, 919, <https://doi.org/10.3390/min10100919>
- Gammons, C.H. and Williams-Jones, A.E. 1997. Chemical mobility of gold in the porphyry-epithermal environment. *Economic Geology*, **92**, 45–59, <https://doi.org/10.2113/gsecongeo.92.1.45>
- Gilio, M., Scambelluri, M., Angel, R. and Alvaro, M. 2021. The contribution of elastic geothermobarometry to the debate on HP v. UHP metamorphism. *Journal of Metamorphic Geology*, **40**, 229–242, <https://doi.org/10.1111/jmg.12625>
- Götze, J. 2009. Chemistry, textures and physical properties of quartz – geological interpretation and technical application. *Mineralogical Magazine*, **73**, 645–671, <https://doi.org/10.1180/minmag.2009.073.4.645>
- Götze, J. and Kempe, U. 2009. Physical Principles of Cathodoluminescence (CL) and its Applications in Geosciences. In: Gucsik, A. (ed.) *Cathodoluminescence and its Application in the Planetary Sciences*. Springer, Berlin, Heidelberg, 1–22, [https://doi.org/10.1007/978-3-540-87529-1\\_1](https://doi.org/10.1007/978-3-540-87529-1_1)
- Götze, J. and Möckel, R. 2012. Quartz: Deposits, Mineralogy and Analytics. Springer Berlin, Heidelberg, <https://doi.org/10.1007/978-3-642-22161-3>
- Götze, J., Plötze, M. and Habermann, D. 2001. Origin, spectral characteristics and practical applications of the cathodoluminescence (CL) of quartz – a review. *Mineralogy and Petrology*, **71**, 225–250, <https://doi.org/10.1007/s007100170040>
- Gregory, M., Lang, J., Gilbert, S. and Hoal, K. 2013. Geometallurgy of the Pebble Porphyry Copper-Gold-Molybdenum Deposit, Alaska: implications for Gold Distribution and Paragenesis. *Economic Geology*, **108**, 463–482, <https://doi.org/10.2113/econgeo.108.3.463>
- Gruner, J. 1922. Paragenesis of the martite ore bodies and magnetites of the Mesabi range [Minnesota]. *Economic Geology*, **17**, 1–14, <https://doi.org/10.2113/gsecongeo.17.1.1>
- Haerberlin, Y., Moritz, R., Fontbote, L. and Cosca, M. 2004. Carboniferous Orogenic Gold Deposits at Patataz, Eastern Andean Cordillera, Peru: geological and structural framework, paragenesis, alteration, and <sup>40</sup>Ar/<sup>39</sup>Ar Geochronology. *Economic Geology*, **99**, 73–112, <https://doi.org/10.2113/gsecongeo.99.1.73>
- Hagni, R. and Grawe, O. 1964. Mineral paragenesis in the Tri-State District, Missouri, Kansas, Oklahoma. *Economic Geology*, **99**, 73–112.
- Hastie, E., Kontak, D. and Lafrance, B. 2020. Gold Remobilization: Insights from Gold Deposits in the Archean Swayze Greenstone Belt, Abitibi Subprovince, Canada. *Economic Geology*, **115**, 241–277, <https://doi.org/10.5382/econgeo.4709>
- Heilbronner, R. and Bruhn, D. 1998. The influence of three-dimensional grain size distributions on the rheology of polyphase rocks. *Journal of Structural Geology*, **20**, 695–707, [https://doi.org/10.1016/S0191-8141\(98\)00010-8](https://doi.org/10.1016/S0191-8141(98)00010-8)
- Hemley, J. and Jones, W. 1964. Chemical aspects of hydrothermal alteration with emphasis on hydrogen

- metasomatism. *Economic Geology*, **59**, 538–569, <https://doi.org/10.2113/gsecongeo.59.4.538>
- Higgins, N. 1985. Wolframite deposition in a hydrothermal vein system; the Grey River tungsten prospect, Newfoundland, Canada. *Economic Geology*, **80**, 1297–1327, <https://doi.org/10.2113/gsecongeo.80.5.1297>
- Hu, H., Li, J., Lentz, D., Ren, Z., Zhao, X., Deng, X. and Hall, D. 2014. Dissolution–reprecipitation process of magnetite from the Chengchao iron deposit: Insights into ore genesis and implication for in-situ chemical analysis of magnetite. *Ore Geology Reviews*, **57**, 393–405, <https://doi.org/10.1016/j.oregeorev.2013.07.008>
- Huston, D. and Large, R. 1989. A chemical model for the concentration of gold in volcanogenic massive sulphide deposits. *Ore Geology Reviews*, **4**, 171–200, [https://doi.org/10.1016/0169-1368\(89\)90017-6](https://doi.org/10.1016/0169-1368(89)90017-6)
- Huston, D., Bottrill, R. *et al.* 1992. Geologic and geochemical controls on the mineralogy and grain size of gold-bearing phases, eastern Australian volcanic-hosted massive sulfide deposits. *Economic Geology*, **87**, 542–563, <https://doi.org/10.2113/gsecongeo.87.3.542>
- Imai, A. 1999. Pyrite Disease in Luzonite from the Lepanto Cu–Au Deposit, Mankayan, Philippines: further example of disease texture and its origin. *Resource Geology*, **49**, 163–168, <https://doi.org/10.1111/j.1751-3928.1999.tb00042.x>
- Imai, A. 2000. Mineral Paragenesis, Fluid Inclusions and Sulfur Isotope Systematics of the Lepanto Far Southeast Porphyry Cu–Au Deposit, Mankayan, Philippines. *Resource Geology*, **50**, 151–168, <https://doi.org/10.1111/j.1751-3928.2000.tb00065.x>
- Ixer, R., Patrick, R. and Stanley, C. 1997. Geology, mineralogy and genesis of gold mineralization at Calliachar–Ular Burn, Scotland. *Transactions of the Institution of Mining and Metallurgy Section B – Applied Earth Science*, **106**, 99–108.
- Jacques, J.M. and Reavy, R.J. 1994. Caledonian plutonism and major lineaments in the SW Scottish Highlands. *Journal of the Geological Society, London*, **151**, 955–969, <https://doi.org/10.1144/gsjgs.151.6.0955>
- Kamilli, R.J. 1998. Paragenesis. In: Marshall, C.P. and Fairbridge, R.W. (eds) *Encyclopedia of Geochemistry*. Springer, Dordrecht, 485–488, [https://doi.org/10.1007/1-4020-4496-8\\_240](https://doi.org/10.1007/1-4020-4496-8_240)
- Kelly, W. and Turneaure, F. 1970. Mineralogy, paragenesis and geothermometry of the tin and tungsten deposits of the eastern Andes, Bolivia. *Economic Geology*, **65**, 609–680, <https://doi.org/10.2113/gsecongeo.65.6.609>
- Keys, M. 1940. Paragenesis in the Hollinger veins. *Economic Geology*, **35**, 611–628, <https://doi.org/10.2113/gsecongeo.35.5.611>
- Köhler, A. 1894. New method of illumination for photomicrographical purposes. *Journal of the Royal Microscopical Society*, **14**, 261–262.
- Lanari, P., Vidal, O., De Andrade, V., Dubacq, B., Lewin, E., Grosch, E. and Schwartz, S. 2014. XMapTools: a MATLAB®-based program for electron microprobe X-ray image processing and geothermobarometry. *Computers & Geosciences*, **62**, 227–240, <https://doi.org/10.1016/j.cageo.2013.08.010>
- Landtwing, M.R. and Pettke, T. 2005. Relationships between SEM-cathodoluminescence response and trace-element composition of hydrothermal vein quartz. *American Mineralogist*, **90**, 122–131, <https://doi.org/10.2138/am.2005.1548>
- Leach, D., Bradley, D., Lewchuk, M., Symons, D., de Marsily, G. and Brannon, J. 2001. Mississippi Valley-type lead–zinc deposits through geological time: implications from recent age-dating research. *Mineralium Deposita*, **36**, 711–740, <https://doi.org/10.1007/s001260100208>
- Lebrun, E., Thébaud, N., Miller, J., Roberts, M. and Evans, N. 2016. Mineralisation footprints and regional timing of the world-class Siguiro orogenic gold district (Guinea, West Africa). *Mineralium Deposita*, **52**, 539–564, <https://doi.org/10.1007/s00126-016-0684-6>
- Lee, A.L., Lloyd, G.E., Torvela, T. and Walker, A.M. 2020. Evolution of a shear zone before, during and after melting. *Journal of the Geological Society*, **177**, 738–751, <https://doi.org/10.1144/jgs2019-114>
- Legros, H., Marignac, C. *et al.* 2016. Detailed paragenesis and Li–mica compositions as recorders of the magmatic-hydrothermal evolution of the Maoping W–Sn deposit (Jiangxi, China). *Lithos*, **264**, 108–124, <https://doi.org/10.1016/j.lithos.2016.08.022>
- Li, J. and Vasconcelos, P. 2002. Cenozoic continental weathering and its implications for the palaeoclimate: evidence from 40Ar/39Ar geochronology of supergene K–Mn oxides in Mt Tabor, central Queensland, Australia. *Earth and Planetary Science Letters*, **200**, 223–239, [https://doi.org/10.1016/S0012-821X\(02\)00594-0](https://doi.org/10.1016/S0012-821X(02)00594-0)
- Li, R., Wang, X., Yang, L., Zhang, B., Liu, Q. and Liu, D. 2020. The characteristic of microstructural deformation of gold bearing pyrite in Jiaodong: the links between nanoscale gold enrichment and crystal distortion. *Ore Geology Reviews*, **122**, 103495, <https://doi.org/10.1016/j.oregeorev.2020.103495>
- Li, H., Wang, Q., Wenig, W., Dong, C., Yang, L., Wang, X. and Deng, J. 2022. Co-precipitation of gold and base metal sulfides during fluid boiling triggered by fault-valve processes in orogenic gold deposits. *Ore Geology Reviews*, **149**, <https://doi.org/10.1016/j.oregeorev.2022.105090>
- Liu, J., Wang, A. *et al.* 2010. Cracking mechanisms during galena mineralization in a sandstone-hosted lead–zinc ore deposit: case study of the Jinding giant sulfide deposit, Yunnan, SW China. *Mineralium Deposita*, **45**, 567–582, <https://doi.org/10.1007/s00126-010-0294-7>
- Lyell, C. 1833. *Principles of Geology, Being an Attempt to Explain the Former Changes of the Earth's Surface, by Reference to Causes now in Operation*. Vol. 1. J. Kay, jun. & brother, Murray, London.
- Machel, H.G. 2000. Application of Cathodoluminescence to Carbonate Diagenesis. In: Pagel, M., Barbin, V., Blanc, P. and Ohnenstetter, D. (eds) *Cathodoluminescence in Geosciences*. Springer, Berlin, Heidelberg, [https://doi.org/10.1007/978-3-662-04086-7\\_11](https://doi.org/10.1007/978-3-662-04086-7_11)
- Mansurbeg, H., El-Ghali, M., Shahrokhi, S., Reif, J., Hussein, H. and Morad, S. 2020. Paragenesis of secondary Ca–Al silicates during hydrothermal alteration of Proterozoic granitic rocks (SE Sweden). *Geological Journal*, **56**, 2135–2147, <https://doi.org/10.1002/gj.4044>
- Mark, F.D., Rice, C.M., Fallick, A.E., Trewin, N.H., Lee, M.R., Boyce, A. and Lee, J.K.W. 2011. <sup>40</sup>Ar/<sup>39</sup>Ar

## Textural mapping and building a paragenetic interpretation

- dating of hydrothermal activity, biota and gold mineralization in the Rhynie hot-spring system, Aberdeenshire, Scotland. *Geochimica et Cosmochimica Acta*, **75**, 555–569, <https://doi.org/10.1016/j.gca.2010.10.014>
- Mark, D.F., Rice, C.M., Hole, M. and Condon, D. 2020. Multi-chromometer dating of the Souter Head complex: rapid exhumation terminates the Grampian Event of the Caledonian Orogeny. *Earth and Environmental Science Transactions of the Royal Society of Edinburgh*, **111**, 95–108, <https://doi.org/10.1017/S1755691020000043>
- Marshall, D.J. 1988. *Cathodoluminescence of Geological Materials*. Unwin Hyman, Boston.
- Martínez-Abad, I., Cepedal, A., Arias, D. and Fuertes-Fuente, M. 2015. The Au–As (Ag–Pb–Zn–Cu–Sb) vein-disseminated deposit of Arcos (Lugo, NW Spain): mineral paragenesis, hydrothermal alteration and implications in invisible gold deposition. *Journal of Geochemical Exploration*, **151**, 1–16, <https://doi.org/10.1016/j.gexplo.2014.11.019>
- Mathieu, L. 2018. Quantifying hydrothermal alteration: a review of methods. *Geosciences*, **8**, <https://doi.org/10.3390/geosciences8070245>
- McLimans, R.K., Barnes, H.L. and Ohmoto, H. 1980. Sphalerite of the Upper Mississippi Valley zinc-lead district, Southwest Wisconsin. *Economic Geology*, **75**, 351–361, <https://doi.org/10.2113/gsecongeo.75.3.351>
- McMullan, D. 2006. Scanning electron microscopy 1928–1965. *Scanning*, **17**, 175–185, <https://doi.org/10.1002/sca.4950170309>
- Mehrabi, B., Tale Fazel, E. and Yardley, B. 2019. Ore geology, fluid inclusions and O-S stable isotope characteristics of Shurab Sb-polymetallic vein deposit, eastern Iran. *Geochemistry*, **79**, 307–322, <https://doi.org/10.1016/j.geoch.2018.12.004>
- Mills, S., Tomkins, A., Weinberg, R. and Fan, H. 2015. Implications of pyrite geochemistry for gold mineralisation and remobilisation in the Jiaodong gold district, northeast China. *Ore Geology Reviews*, **71**, 150–168, <https://doi.org/10.1016/j.oregeorev.2015.04.022>
- Monteiro, L., Xavier, R., de Carvalho, E., Hitzman, M., Johnson, C., de Souza Filho, C. and Torresi, I. 2007. Spatial and temporal zoning of hydrothermal alteration and mineralization in the Sossego iron oxide–copper–gold deposit, Carajás Mineral Province, Brazil: paragenesis and stable isotope constraints. *Mineralium Deposita*, **43**, 129–159, <https://doi.org/10.1007/s00126-006-0121-3>
- Mookherjee, A. 1964. The geology of the Zawar lead-zinc mine, Rajasthan, India. *Economic Geology*, **59**, 656–677, <https://doi.org/10.2113/gsecongeo.59.4.656>
- Moura, M., Botelho, N., Olivo, G., Kyser, K. and Pontes, R. 2014. Genesis of the Proterozoic Mangabeira tin–indium mineralization, Central Brazil: evidence from geology, petrology, fluid inclusion and stable isotope data. *Ore Geology Reviews*, **60**, 36–49, <https://doi.org/10.1016/j.oregeorev.2013.12.010>
- Müller, A. and Ehle, H. 2021. Rapid ore classification for real-time mineral processing optimisation at the Niederschlag multi-generation hydrothermal barite-fluorite vein deposit, Germany. *Mineralium Deposita*, **56**, 417–424, <https://doi.org/10.1007/s00126-020-01037-w>
- Myint, A., Li, H., Mitchell, A., Selby, D. and Wagner, T. 2021. Geology, mineralogy, ore paragenesis, and molybdenite Re–Os geochronology of Sn–W (–Mo) mineralization in Padatgyaung and Dawei, Myanmar: implications for timing of mineralization and tectonic setting. *Journal of Asian Earth Sciences*, **212**, 104725, <https://doi.org/10.1016/j.jseaes.2021.104725>
- Nagase, T. and Kojima, S. 1997. An SEM examination of the chalcopyrite disease texture and its genetic implications. *Mineralogical Magazine*, **61**, 89–97, <https://doi.org/10.1180/minmag.1997.061.404.09>
- Neilson, J.C., Kokelaar, B.P. and Crowley, Q.G. 2009. Timing, relations and cause of plutonic and volcanic activity of the Siluro-Devonian post-collision magmatic episode in the Grampian Terrane, Scotland. *Journal of the Geological Society, London*, **166**, 545–561, <https://doi.org/10.1144/0016-76492008-069>
- Newhouse, W. 1927. Intimate intergrowths and mutual boundaries as proof of contemporaneous deposition. *Economic Geology*, **22**, 403–407, <https://doi.org/10.2113/gsecongeo.22.4.403>
- Niedrig, H. 1978. Physical background of electron backscattering. *The Journal of Scanning Microscopies*, **1**, 17–34, <https://doi.org/10.1002/sca.4950010103>
- Nuttall, R.H. 1979. Andrew Pritchard's contribution to Metallurgical Microscopy. *Technology and Culture*, **20**, 569, <https://doi.org/10.2307/3103817>
- Oldenbourg, R. 2013. Polarized light microscopy: principles and practice. *Cold Spring Harbour Protocols*, **11**, <https://doi.org/10.1101/pdb.top078600>
- Oliver, G.J.H. 2001. Reconstruction of the Grampian episode in Scotland: its place in the Caledonian Orogeny. *Tectonophysics*, **332**, 23–49, [https://doi.org/10.1016/S0040-1951\(00\)00248-1](https://doi.org/10.1016/S0040-1951(00)00248-1)
- Oliver, G., Wilde, S. and Wan, Y. 2008. Geochronology and geodynamics of Scottish granitoids from the late Neoproterozoic break-up of Rodinia to Palaeozoic collision. *Journal of the Geological Society*, **165**, 661–674, <https://doi.org/10.1144/0016-76492007-105>
- Parnell, J., Earls, G. *et al.* 2000. Regional fluid flow and gold mineralization in the Dalradian of the Sperrin Mountains, Northern Ireland. *Economic Geology*, **95**, 1389–1416, <https://doi.org/10.2113/gsecongeo.95.7.1389>
- Patrick, R.A.D. 1984. Sulphide mineralogy of the Tomnadashan copper deposit and the Corrie Buie lead veins, south Loch Tayside, Scotland. *Mineralogical Magazine*, **48**, 85–91.
- Patrick, R.A.D., Boyce, A. and MacIntyre, R.M. 1988. Gold-silver vein mineralisation at Tyndrum, Scotland. *Mineralogy and Petrology*, **38**, 61–76, <https://doi.org/10.1007/BF01162482>
- Perret, J., Andre-Mayer, A-S. *et al.* 2021. Structural and geochemical ore-forming processes in deformed gold deposits: towards a multiscale and multimethod approach. *Geological Society, London, Special Publications*, **516**, <https://doi.org/10.1144/SP516-2021-37>
- Pittarello, L., Pennacchioni, G. and Di Toro, G. 2012. Amphibolite-facies pseudotachylytes in Premosello metagabbro and felsic mylonites (Ivrea Zone, Italy). *Tectonophysics*, **580**, 43–57, <https://doi.org/10.1016/j.tecto.2012.08.001>
- Plumlee, G. and Whitehouse-Veaux, P. 1994. Mineralogy, paragenesis, and mineral zoning of the Bulldog

- Mountain vein system, Creede District, Colorado. *Economic Geology*, **89**, 1883–1905, <https://doi.org/10.2113/gsecongeo.89.8.1883>
- Pumpelly, R. 1871. The paragenesis and derivation of copper and its associates on Lake Superior. *American Journal of Science*, **s3–2**, 188–198, <https://doi.org/10.2475/ajs.s3-2.9.188>
- Quilichini, A., Siebenaller, L., Teyssier, C. and Venne-mann, T. 2016. Magmatic and meteoric fluid flow in the Bitterroot extensional detachment shear zone (MT, USA) from ductile to brittle conditions. *Journal of Geodynamics*, **101**, 109–128, <https://doi.org/10.1016/j.jog.2016.05.006>
- Randive, K., Harri, K., Dora, M., Malpe, D. and Bhondwe, A. 2022. Study of fluid inclusions: methods, techniques and applications. *Gondwana Geological Magazine*, **29**, 19–28.
- Ray, J. 1914. Paragenesis of the ore minerals in the Butte District, Montana. *Economic Geology*, **9**, 463–481, <https://doi.org/10.2113/gsecongeo.9.5.463>
- Reed, R. and Milliken, K. 2003. How to overcome imaging problems associated with carbonate minerals on SEM-based cathodoluminescence systems. *Journal of Sedimentary Research*, **73**, 328–332, <https://doi.org/10.1306/081002730328>
- Rice, C.M., Ashcroft, W.A. *et al.* 1995. A Devonian auriferous hot spring system, Rhynie, Scotland. *Journal of the Geological Society, London*, **152**, 229–250, <https://doi.org/10.1144/gsjgs.152.2.0229>
- Rice, C., Mark, D., Selby, D., Neilson, J. and Davidheiser-Kroll, B. 2016. Age and geologic setting of quartz vein-hosted gold mineralization at Curraghinalt, Northern Ireland: implications for genesis and classification. *Economic Geology*, **111**, 127–150, <https://doi.org/10.2113/econgeo.111.1.127>
- Richardson, C. and Pinckney, D. 1984. The chemical and thermal evolution of the fluids in the Cave-in-Rock fluorspar district, Illinois; mineralogy, paragenesis, and fluid inclusions. *Economic Geology*, **79**, 1833–1856, <https://doi.org/10.2113/gsecongeo.79.8.1833>
- Roberts, J.L. and Treagus, J.E. 1977. Polyphase generation of nappe structures in the Dalradian rocks of the southwest Highlands of Scotland. *Scottish Journal of Geology*, **13**, 237–254, <https://doi.org/10.1144/sjg13030237>
- Rochow, T.G. and Tucker, P.A. 1994. *Introduction to Microscopy by Means of Light, Electrons, X Rays, or Acoustics*. Springer, Boston, [https://doi.org/10.1007/978-1-4899-1513-9\\_1](https://doi.org/10.1007/978-1-4899-1513-9_1)
- Rogowitz, A., Zaefferer, S. and Dubosq, R. 2018. Direct observation of dislocation nucleation in pyrite using combined electron channelling contrast imaging and electron backscatter diffraction. *Terra Nova*, **30**, 423–430, <https://doi.org/10.1111/ter.12358>
- Rubatto, D., Müntener, O., Barnhoorn, A. and Gregory, C. 2008. Dissolution-reprecipitation of zircon at low-temperature, high-pressure conditions (Lanzo Massif, Italy). *American Mineralogist*, **93**, 1519–1529, <https://doi.org/10.2138/am.2008.2874>
- Sahoo, P. and Venkatesh, A. 2015. Constraints of mineralogical characterization of gold ore: implication for genesis, controls and evolution of gold from Kundarkocha gold deposit, eastern India. *Journal of Asian Earth Sciences*, **97**, 136–149, <https://doi.org/10.1016/j.jseas.2014.09.040>
- Sanderson, J. 2019. *Understanding Light Microscopy*. John Wiley and Sons.
- Schwartz, G. 1959. Hydrothermal alteration. *Economic Geology*, **54**, 161–183, <https://doi.org/10.2113/gsecongeo.54.2.161>
- Shaw, J., Torvela, T., Cooper, M.R., Leslie, A. and Chapman, R. 2022. A progressive model for the development of the Cavanacaw Au–Ag–Pb vein deposit, Northern Ireland, and implications for the evolution and metallogeny of the Grampian Terrane. *Journal of Structural Geology*, **161**, 104637, <https://doi.org/10.1016/j.jsg.2022.104637>
- Shore, M. and Fowler, A. 1996. Oscillatory zoning in minerals; a common phenomenon. *Canadian Mineralogist*, **31**, 1111–1126.
- Sibson, R.H. 1994. Crustal stress, faulting and fluid flow. *Geological Society, London, Special Publications*, **78**, 69–84.
- Sims, P. 1956. Paragenesis and structure of pitchblende-bearing veins, Central City District, Gilpin County, Colorado. *Economic Geology*, **51**, 739–756, <https://doi.org/10.2113/gsecongeo.51.8.739>
- Slack, J. 1980. Multistage vein ores of the Lake City District, western San Juan Mountains, Colorado. *Economic Geology*, **75**, 963–991, <https://doi.org/10.2113/gsecongeo.75.7.963>
- Soloviev, S. and Kryazhev, S. 2018. Magmatic-hydrothermal evolution at the Lyangar redox-intermediate tungsten-molybdenum skarn deposit, western Uzbekistan, Tien Shan: insights from igneous petrology, hydrothermal alteration, and fluid inclusion study. *Lithos*, **316–317**, 154–177, <https://doi.org/10.1016/j.lithos.2018.07.015>
- Soper, N.J., Ryan, P.D. and Dewey, J.F. 1999. Age of the Grampian Orogeny in Scotland and Ireland. *Journal of the Geological Society, London*, **156**, 1231–1236, <https://doi.org/10.1144/gsjgs.156.6.1231>
- Spence-Jones, C., Jenkin, G., Boyce, A., Hill, N. and Sangster, C. 2018. Tellurium, magmatic fluids and orogenic gold: an early magmatic fluid pulse at Cononish gold deposit, Scotland. *Ore Geology Reviews*, **102**, 894–905, <https://doi.org/10.1016/j.oregeorev.2018.05.014>
- Steno, N. 1669. De solido intra solidum naturaliter contento Dissertationis prodromus. Ex typographia sub signo Stellae.
- Stephenson, D., Mendum, J., Fettes, D. and Leslie, A. 2013. The Dalradian rocks of Scotland: an introduction. *Proceedings of the Geologists' Association*, **124**, 3–82, <https://doi.org/10.1016/j.pgeola.2012.06.002>
- Stevens-Kalceff, M. 2009. Cathodoluminescence micro-characterization of point defects in  $\alpha$ -quartz. *Mineralogical Magazine*, **73**, 585–605, <https://doi.org/10.1180/minmag.2009.073.4.585>
- Sykora, S., Cooke, D. *et al.* 2018. Evolution of pyrite trace element compositions from porphyry-style and epithermal conditions at the Lihir Gold Deposit: implications for ore genesis and mineral processing. *Economic Geology*, **113**, 193–208, <https://doi.org/10.5382/econgeo.2018.4548>
- Tadesse, S. 2004. Genesis of the Shear Zone-related Gold Vein Mineralization of the Lega Dembi Gold Deposit, Adola Gold Field, Southern Ethiopia. *Gondwana*

## Textural mapping and building a paragenetic interpretation

- Research*, **7**, 481–488, [https://doi.org/10.1016/S1342-937X\(05\)70799-1](https://doi.org/10.1016/S1342-937X(05)70799-1)
- Tanner, P.W.G. 2014a. A kinematic model for the Grampian Orogeny, Scotland. *Geological Society, London, Special Publications*, **390**, 467–511.
- Tanner, P. 2014b. Structural controls and origin of gold–silver mineralization in the Grampian Terrane of Scotland and Ireland. *Geological Magazine*, **151**, 1072–1094, <https://doi.org/10.1017/S0016756813001131>
- Tanner, P., Thomas, C., Harris, A., Gould, D., Harte, B., Treagus, J. and Stephenson, D. 2013. The Dalradian rocks of the Highland Border region of Scotland. *Proceedings of the Geologists' Association*, **124**, 215–262, <https://doi.org/10.1016/j.pgeola.2012.07.013>
- Taylor, H. 1974. The Application of Oxygen and Hydrogen Isotope Studies to Problems of Hydrothermal Alteration and Ore Deposition. *Economic Geology*, **69**, 843–883, <https://doi.org/10.2113/gsecongeo.69.6.843>
- Taylor, R., Monecke, T., Reynolds, T. and Monecke, J. 2021. Paragenesis of an Orogenic Gold Deposit: new insights on mineralizing processes at the Grass Valley District, California. *Economic Geology*, **116**, 323–356, <https://doi.org/10.5382/econgeo.4794>
- Tchalenko, J.S. 1970. Similarities between Shear Zones of Different Magnitudes. *GSA Bulletin*, **81**, 1625–1640, [https://doi.org/10.1130/0016-7606\(1970\)81\[1625:SBSZOD\]2.0.CO;2](https://doi.org/10.1130/0016-7606(1970)81[1625:SBSZOD]2.0.CO;2)
- Thomas, H., Large, R. *et al.* 2011. Pyrite and Pyrrhotite Textures and Composition in Sediments, Laminated Quartz Veins, and Reefes at Bendigo Gold Mine, Australia: insights for Ore Genesis. *Economic Geology*, **106**, 1–31, <https://doi.org/10.2113/econgeo.106.1.1>
- Torvela, T. and Kurhila, M. 2022. Timing of syn-orogenic, high-grade transtensional shear zone formation in the West Uusimaa Complex, Finland. *Bulletin of the Geological Society of Finland*, **94**, 5–22, <https://doi.org/10.17741/bgsf/94.1.001>
- Treagus, J. 2003. The Loch Tay Fault: type section geometry and kinematics. *Scottish Journal of Geology*, **39**, 135–144, <https://doi.org/10.1144/sjg39020135>
- Treagus, J.E., Patrick, R.A.D. and Curtis, S.F. 1999. Movement and mineralization in the Tyndrum fault zone, Scotland and its regional significance. *Journal of the Geological Society, London*, **156**, 591–604, <https://doi.org/10.1144/gsjgs.156.3.0591>
- van Ryt, M., Sanislav, I., Dirks, P., Huizenga, J., Mturi, M. and Kolling, S. 2017. Alteration paragenesis and the timing of mineralised quartz veins at the world-class Geita Hill gold deposit, Geita Greenstone Belt, Tanzania. *Ore Geology Reviews*, **91**, 765–779, <https://doi.org/10.1016/j.oregeorev.2017.08.023>
- Vaughan, D. and Ixer, R. 1980. Studies of sulphide mineralogy of north Pennine ores and its contribution to genetic models. *Transactions of the Institution of Mining and Metallurgy, Section B, Applied Earth Science*, **89**, 99–109.
- Vidal, O., De Andrade, V., Lewin, E., Munoz, M., Parra, T. and Pascarelli, S. 2006. P-T-deformation-Fe3 + /Fe2+ mapping at the thin section scale and comparison with XANES mapping: application to a garnet-bearing metapelite from the Sambagawa metamorphic belt (Japan). *Journal of Metamorphic Geology*, **24**, 669–683, <https://doi.org/10.1111/j.1525-1314.2006.00661.x>
- Wang, D., Zhen, S. *et al.* 2021. Mineral paragenesis and hydrothermal evolution of the Dabaiyang tellurium-gold deposit, Hebei Province, China: constraints from fluid inclusions, H-O-He-Ar isotopes, and physico-chemical conditions. *Ore Geology Reviews*, **130**, 103904, <https://doi.org/10.1016/j.oregeorev.2020.103904>
- Wangen, M. and Munz, I. 2004. Formation of quartz veins by local dissolution and transport of silica. *Chemical Geology*, **209**, 179–192, <https://doi.org/10.1016/j.chemgeo.2004.02.011>
- Wei, Y., Yang, L., Feng, J., Wang, H., Lv, G., Li, W. and Liu, S. 2019. Ore-Fluid Evolution of the Sizhuang Orogenic Gold Deposit, Jiaodong Peninsula, China. *Minerals*, **9**, <https://doi.org/10.3390/min9030190>
- Wilkinson, J.J. and Johnston, J.D. 1996. Pressure fluctuations, phase separation, and gold precipitation during seismic fracture propagation. *Geology*, **24**, 395–398, [https://doi.org/10.1130/0091-7613\(1996\)024<0395:PFPSAG>2.3.CO;2](https://doi.org/10.1130/0091-7613(1996)024<0395:PFPSAG>2.3.CO;2)
- Wilkinson, J., Boyce, A., Earls, G. and Fallick, A. 1999. Gold remobilization by low-temperature brines; evidence from the Curraghinalt gold deposit, Northern Ireland. *Economic Geology*, **94**, 289–296, <https://doi.org/10.2113/gsecongeo.94.2.289>
- Wilson, C. 1994. Crystal growth during a single-stage opening event and its implications for syntectonic veins. *Journal of Structural Geology*, **16**, 1283–1296, [https://doi.org/10.1016/0191-8141\(94\)90070-1](https://doi.org/10.1016/0191-8141(94)90070-1)
- Yang, L., Deng, J. *et al.* 2016. Relationships Between Gold and Pyrite at the Xincheng Gold Deposit, Jiaodong Peninsula, China: implications for Gold Source and Deposition in a Brittle Epizonal Environment. *Economic Geology*, **111**, 105–126, <https://doi.org/10.2113/econgeo.111.1.105>
- Zhu, D., Li, H., Algeo, T., Jiang, W. and Wang, C. 2021. The prograde-to-retrograde evolution of the Huangshaping skarn deposit (Nanling Range, South China). *Mineralium Deposita*, **56**, 1087–1110, <https://doi.org/10.1007/s00126-021-01042-7>